Green Energy Breakthroughs: Nano-Catalysts for Bioenergy Generation, and A Lab-scale Experimental Case Study with Glucose Oxidase (GOx) Enzymatic Nano-Catalysts Coated with Fe_2O_3/SiO_2 Magnetic Nanocomposites

RUKİYE ÖZTEKİN, DELİA TERESA SPONZA*
[a] Department of Environmental Engineering
Dokuz Eylül University
Tınaztepe Campus, 35160 Buca/Izmir,
TURKEY

**Corresponding Author*

Abstract: - Microbial fuel cells and anaerobic digestion are promising bioenergy methods but inefficient and scalable. With its exceptional surface area-to-volume ratio, nano-catalysts are revolutionizing this field. Researchers have improved energy conversion efficiency by immobilizing or embedding nanoparticles on electrodes or catalytic supports to promote electron transport. Nanomaterials like graphene-based catalysts and metal nanoparticles speed up organic matter breakdown and make bioenergy systems more profitable. Researchers are working harder to find new bioenergy-generating methods to address environmental concerns and the demand for sustainable energy. The study discusses how nano-catalysts and enzymatic catalysts are revolutionizing bioenergy production in green energy. Additionally, enzymatic catalysts are the best bioenergy catalysts. Highly specialized, biocompatible, and renewable enzymes provide unrivaled biofuel production potential. Protein engineering and immobilization have improved enzymes for bioenergy systems. Enzymatic catalysts enable biofuel generation from more feedstocks without harsh chemical procedures by controlling biological reactions quickly and precisely. Combining nano-catalysts and enzymatic catalysts is promising. Nano-catalysts improve enzymatic processes by creating a favorable microenvironment, enhancing surface binding sites, and enabling substrate transport. This combination may maximize bioenergy systems' biofuel output and wastewater treatment capabilities. In this study, as a green energy breakthrough a nano-catalysts was used for bioenergy generation. In the lab-scale experimental study from GOx which is an oxidoreductase that catalyses the oxidation of β-D-glucose to D-glucono-δ-lactone with glucose oxidase was coated with hematite/silicon dioxide magnetic nanocomposites (Fe_2O_3/SiO_2 MNCs) and the effects of some experimental conditions on photocatalytic degradation process of enzymatic Gox was investigated. The physicochemical properties of the experimental samples were investigated by XRD, FTIR, FE-SEM, EDX, UV-vis spectra, HRTEM and VSM analyses, respectively. The maximum > 99% photocatalytic degradation yields for GOx were measured at 20 mg/l Fe_2O_3/SiO_2 MNC and 1.0 mg/l GOx enzymatic nano-catalyst concentrations, at 300 W UV-vis light irradiation, after 120 min photodegradation time, at pH=7.0, and at 50ºC, respectively. According to this study, it was found that by integrating the nano-catalysts to the enzymatic catalysts is a green energy breakthrough to detect sustainable energy generation. These advances will improve the bioenergy generation by overcoming current techniques, by opening new sustainable energy production prospects, and expediting our transition to a greener, more sustainable future.

Key-Words: - Anaerobic digestion (AD); Bioenergy generation; Bioenergy systems; Biofuel; Glucose oxidase (GOx) enzymatic nano-catalysts; Green energy breakthroughs; Hematite/silicon dioxide magnetic nanocomposites (Fe_2O_3/SiO_2 MNCs); Microbial fuel cells; Nanomaterials; Sustainable energy production.

Received: June 24, 2025. Revised: October 11, 2025. Accepted: December 12, 2025. Published: March 23, 2026.

1 Introduction

Bioenergy sources are essential to a sustainable energy future since they are carbon-neutral when handled properly. Bioenergy uses the natural carbon cycle to balance carbon dioxide (CO_2) emissions from burning with carbon absorbed during biomass growth (Fig. 1). Bioenergy is appealing in the fight against climate change due to its sustainability, [1], [2]. Modern research and technology show that nano-

catalysts and enzymatic catalysts may alter bioenergy. Utilizing nano-catalysts with the combination of metal oxides like aluminium trioxide (Al_2O_3), iron trioxide (Fe_3O_4), and titanium dioxide (TiO_2), can raise the productivity of biodiesel production, optimize operating conditions, and increase product quality, [3], [4], [5].

* Figure 1 can be found in the Appendix section.

Climate warming and fossil fuel depletion make sustainable energy solutions more important than ever. Innovative technologies and research in green energy generation have created new opportunities for tackling these global issues, [6]. This study examines nano-catalysts and enzymatic catalysts' potential in bioenergy production, a crucial area at the intersection of renewable energy and biotechnology. Enzymatic and nano-catalyst catalysts are essential to the synthesis of bioenergy (Fig. 2). By increasing selectivity, quality, and yield, nanoparticles such as organic and inorganic metals have been utilized to increase the production of biofuels. They have been discovered to be reliable and reasonably priced catalysts for enzyme immobilization, which improves the production of biofuel in microorganisms.

* Figure 2 can be found in the Appendix section.

Sustainable energy is increasingly crucial due to climate change and fossil fuel depletion. Advances in innovative research and technology have propelled the field of green energy generation. This paper examines the remarkable potential of nano-catalysts and enzymatic catalysts in bioenergy production, a hot issue in renewable energy and biotechnology, [7]. Nano-catalysts are precise at the atomic and molecular level, where surface effects dominate catalysis. They might boost solar cell and catalytic converter efficiency, enabling cleaner, more sustainable electricity production. Enzymatic catalysts, inspired by nature's efficiency and selectivity, are revolutionizing biofuel, pharmaceutical, and other industries, [8]. Their green alternatives to traditional chemical processes are driven by accuracy and minimal waste in complex reactions. Nano-catalysts accelerate bioenergy conversion by breaking down complicated organic molecules into energy-rich chemicals. In contrast, enzymatic catalysts operate as molecular scissors, displaying unmatched selectivity as they cut biomass into biofuels, [9].

In the present study, a green energy breakthrough namely nano-catalysts for bioenergy generation were taken into consideration and a lab-scale experimental study was performed from GOx enzymatic nano-catalysts coated with Fe_2O_3/SiO_2 MNCs at different experimental conditions during photocatalytic degradation process. The physicochemical properties of the GOx enzymatic nano-catalysts coated with Fe_2O_3/SiO_2 MNCs samples were investigated by XRD, FTIR, FE-SEM, EDX, UV-vis spectra, HRTEM and VSM analyses. The effects of some operational conditions such as photocatalytic degradation time, temperature, pH values, GOx enzyme / Fe_2O_3/SiO_2 MNCs concentrations on the photocatalytic degradation efficiencies of GOx which is an oxidoreductase catalysing the oxidation of β-D-glucose to D-glucono-δ-lactone were investigated.

1.1 Anaerobic Digestion (AD) Unlocking Bioenergy

AD is a revolutionary technology that can unleash bioenergy resources and handle waste management and environmental issues. This eco-friendly method uses microorganisms to break down organic waste without oxygen (O_2), producing biogas and nutrient-rich digestate. The adaptability of AD is a significant benefit. It processes organic feedstocks such as sewage sludge, agricultural waste, and food waste, [10], [11], [12]. This versatility makes it helpful in managing organic waste, diverting it from landfills, and lowering greenhouse gas emissions. Fig. 3 presents a schematic representation of AD, which liberates bioenergy by catalyzing the degradation of organic waste.

* Figure 3 can be found in the Appendix section.

The anaerobic digestion process is a renewable energy technology that can generate bioenergy from biomass. AD is a complex, multistep procedure where microorganisms break down organic matter in the absence of oxygen, and it produces biogas and biofertilizers as byproducts. At the end of the AD process, biofertilizer in the form of liquid and solid digestate is a useful soil conditioner. It is rich in organic matter and nutrients, making it beneficial for improving soil structure and fertility. The breakdown of complex organic matter involves four stages: hydrolysis, acidogenesis, acetogenesis, and methanogenesis, [13], [14]. As shown in Fig. 4, the first stage of AD is hydrolysis. In this stage, bacteria from the slurry generate hydrolytic enzymes that break down long-chain polymers such as proteins ($C_{13}H_{25}O_7N_3S$), carbohydrates ($C_6H_{12}O_6$), lipids ($C_{12}H_{24}O_6$), and all insoluble polymers into shorter chains like glucose, fatty acids, glycerol, and amino acids.

* Figure 4 can be found in the Appendix section.

Although, these new molecules are soluble and in high concentration, they are not yet fermentable. Therefore, the AD process moves to the second stage, called acidogenesis. In the acidogenesis stage, the monomers or oligomers (e.g., glucose, fatty acids, glycerol, and amino acids) are further broken down into volatile fatty acids (VFAs), acetate, H_2, and CO_2 by anaerobic oxidizers or fermentative bacteria. The process then proceeds to the acetogenesis stage, where acetogenic bacteria convert the VFAs into acetate, H_2, and CO_2. Finally, in the methanogenesis stage, acetate is converted into methane (CH_4) and CO_2 by acetate-oxidizing bacteria/homo acetogenic bacteria. This last step, known as methanogenesis, produces CH_4 as a valuable end product of the AD process, [13], [15], [16], [17]. The digested substrates are full of nutrient-rich biomass, which can be further directly used as a liquid fertilizer for organic farming, [18], [19].

1.1.1 Biogas and Biogas Composition

This biogas primarily consists of CH_4 and CO_2, but also includes minor traces of hydrogen sulfide (H_2S), carbon monoxide (CO), ammonia (NH_3), water vapor [H_2O(g)], nitrogen (N_2), oxygen (O_2), hydrogen (H_2), siloxanes, and hydrocarbons, [15], [20], [21]. The typical composition of biogas is presented in Table 1.

* Table 1 can be found in the Appendix section.

The raw Biogas potential of a specific biodegradable waste can be projected by the Buswell Eq. (1), [22].

$$C_{\alpha_c}H_{\alpha_h}O_{\alpha_o}N_{\alpha_n}S_{\alpha_s} + {}^{1}/_{4}\,(4\alpha_c - \alpha_h - 2\alpha_o + 3\alpha_n + 2\alpha_s)H_2O \xrightarrow{A} {}^{1}/_{8}\,(4\alpha_c - \alpha_h - 2\alpha_o + 3\alpha_n + 2\alpha_s)CH_4 + {}^{1}/_{8}\,(4\alpha_c - \alpha_h - 2\alpha_o + 3\alpha_n + 2\alpha_s)CO_2 + \alpha_n NH_3 + \alpha_s H_2S \quad (1)$$

where, the Greek letter (α) denotes the moles of elements in the feedstock's chemical formula: α_c for carbon, α_h for hydrogen, α_o for oxygen, α_n for nitrogen, and α_s for sulfur.

1.1.2 Factors Affecting Biogas Generation

The AD process occurs in a digester and the efficiency of digesters in generating raw biogas or the potential yield of methane is influenced by various physical, biological, and chemical factors. These factors consist of the organic waste (structure of the feedstock and particle size), hydraulic retention time (HRT), stirring speed, carbon/nitrogen (C/N) ratio, pH, temperature, organic loading rate (OLR), [23]. These factors will directly influence the raw biogas generation cycle and contribute to changes in the surrounding environmental conditions and the activities of the bacterial community within the digester, [15]. The controlling constraints that optimize CH_4 yield in terms of quantity and quality are as follows.

1.1.2.1 pH

The pH value measures the acidity or alkalinity of a sample, expressed as the logarithm of the reciprocal of the hydrogen ion (H^+) concentration in gram equivalents per liter of the solution. For optimal bacterial growth during all stages of the AD process, the pH of the substrate slurry should be maintained between 6.5 and 7.5, [21], [24]. The pH of the slurry is influenced by factors such as CO_2 levels, VFAs, and temperature, [25]. According to Yadvika et al., [26], a pH range between 5.0 and 7.5 can result in an increased methane yield up to 75% as compared to the conventional pH range.

1.1.2.2 Temperature

Temperature is one of the major affecting parameters in the AD process, which significantly impacts bacterial activity from the initial hydrolysis stage, [27]. The AD process typically operates within two temperature ranges: mesophilic (32–42°C) and thermophilic (48–55°C), [14], [28]. While higher temperatures can increase biogas production, they often result in lower methane yields and higher CO_2 percentages, reducing the calorific value of the biogas, [24]. The optimal temperature for efficient and continuous biogas production is found to be between 32°C and 35°C, [24]. If the temperature drops below 25°C, biogas production decreases, and at 10°C, it stops entirely. Additionally, odour problems and pathogen reduction can be solved by maintaining the temperature range of 48°C–55°C, [24].

1.1.2.3 OLR

The OLR represents the amounts of organic substrates added to a digester per day per unit volume, [14], [23]. This key factor impacts the raw biogas production rate because it is directly dependent on the volatile solids (VS) of the substrates, [24]. A lower OLR generally produces more bio-methane yield, [26], because of the gradual decomposition of organic matter. Optimal feeding rates of feedstock to a digester support the boost of raw biogas production, but beyond that, the raw biogas yield remains constant, [29]. Generally,

optimal values of OLR and yield of CH_4 are reported in Table 2.

* Table 2 can be found in the Appendix section.

OLR is calculated with the help of Eq. (2), [30].

$$OLR = \frac{S}{RT} - \frac{[Q]*[S]}{V} \quad (2)$$

where *OLR*: signifies organic loading rate (kg feedstock/m^3 digester/ day), *RT*: Retention time (days), *S*: represents feedstock concentration in total volatile solid (TVS), *V*: for a volume of the digester (m^3), *Q*: means flow rate of the slurry (m^3/day).

1.1.2.4 Organic waste: (structure of feedstock & particle size)

The potential yield of CH_4 is generally calculated based on the initial characteristics of the selected organic waste feedstock, [30]. Different substrates show distinct characteristics, which are highlighted in Table 3.

* Table 3 can be found in the Appendix section.

At the initial stage of biogas production, it is essential to identify the biomethane potential (BMP) of the substrates. This is achieved through laboratory tests, such as the fermentation test GB_{21} and the BMP test, [30]. This selection is critical for maximizing biogas yield and ensuring the efficiency and stability of the digestion process. The particle size of the feedstock is not as critical as temperature or pH in the AD, but it still affects biogas production. If the substrate size is too large, it can clog the digester, making it difficult for microbes to digest the feedstock efficiently, which can lead to reduced biogas production, [26]. Conversely, smaller particles provide a greater surface area for microbes, enhancing microbial activity and boosting biogas generation, [29]. According to, Yadvika et al., [26], most biogas was produced from feedstock with particle sizes of 0.088 mm and 0.40 mm, out of the five sizes tested: 0.40, 0.088, 1.0, 3.0, 6.0 mm, respectively. Physical pretreatment, such as grinding, significantly reduces the size of the feedstock, [31].

1.1.2.5 HRT

HRT is the average time for which the decomposable substrate slurry remains inside the digester before it is removed from the digester, [26]. HRT is affected by the type of solid substrates and temperature inside the digester, [24]. Generally, in tropical countries, HRT varies from 30 to 50 days while in colder countries it may go up to 100 days, [26]. In India, the HRT is 10–14 days when the temperature of the digester is in the range of mesophilic, and for the thermophilic range it is 14 days [14]. Optimizing the HRT for biogas plants is necessary because a low HRT risks washout of the active microbial bacteria population and a long HRT require a large volume for the digester and hence a greater capital cost, [26]. According to, Sanchez et al., [32], increasing the HRT improved the removal of substrate slurry when treating cattle manure. Desai and Madamwar, [40] reported the highest raw biogas production of 2.2 l/l/day with 62% of CH_4 yield at an HRT of 10 days and a loading rate of 6 gm TS/l while treating a mix of cattle manure, poultry waste, and cheese whey in a 2/1/3 ratio.

1.1.2.6 Stirring speed

Stirring speed, also known as agitation, is a crucial factor in the AD process. It causes the substrate slurry to rotate inside the digester, enhancing BMP, [24], [26]. Stirring speed largely depends on the design of the blade and the viscosity of the slurry. Proper agitation prevents the substrate from settling down and forming scum, [24]. In a study examining various stirring speeds (30, 40, 50, 60, and 70 rpm), it was found that the highest raw biogas production was achieved at 30 rpm, [34]. It has been determined that slow speeds of stirring are most effective for increasing raw biogas and CH_4 yield, [14]. According to Yadvika et al. [26], the methane yield can be enhanced by physically disrupting cellular substrates. However, optimum stirring speed also depends on the digester size and volume of the substrate in the digester.

1.1.2.7 C/N ratio

C/N ratio is the ratio of the carbon and nitrogen compounds in substrates. It is the key factor for the AD process because it helps to maintain a steady AD process by adding the co-substrates into the AD process, [30]. Generally, the ideal C/N ratio for the AD process is in the range of 20–23, [35]. Some of the various organic waste C/N ratio is mentioned in Table 4.

* Table 4 can be found in the Appendix section.

If the C/N ratio is less than 25, the raw biogas production is detected to be low and if it is greater than 25, it will lead to the generation of toxic gases such as NH_3, [14]. The N_2 in an AD reactor primarily comes from proteins and is essential for microbial growth. If the C/N ratio is too low, as a result, NH_3 can build which disturbs the raw biogas and yield of CH_4 production and it helps to potentially leads to

process failure, [23]. Adding feedstock like agricultural waste or paper waste can significantly raise the carbon content in the substrates, which helps to prevent these issues [36]. According to, Zeshan et al. [37], increasing the C/N ratio from 27 to 32 by mixing green waste, food waste, and paper waste reduces the NH_3 content by approximately 30%.

1.2 Challenging the Notion of Sustainability

Challenging the concept of sustainability, previously seen as a beacon of hope for human-environment harmony, means confronting rising problems and questions today. This paradigm shift recognizes that our present path may not meet the intended sustainability ideals. Environmental strain is a significant sustainability concern, [38], [39]. Human activity's substantial influence on Earth's natural systems is shown through climate change, resource depletion, and ecological deterioration. This realization has made us question whether our existing economic and industrial strategies, which prioritize short-term benefits above environmental health, are sustainable.

1.3 Nano-catalysts Transforming Bioenergy

Bioenergy from biomass and waste is essential to a sustainable electricity future. However, conventional bioenergy production systems generally struggle with efficiency, resource consumption, and environmental effects, [40]. Bioenergy processes have been transformed by nano-catalysts in recent years, presenting the possibility to overcome these limits and revolutionize the area. Due to, their large surface area-to-volume ratios and specific surface reactivity, nano-catalysts are highly catalytic. These traits make them helpful in accelerating chemical processes, including bioenergy generation.

Bioenergy techniques using nano-catalysts improve biomass conversion and biofuel generation (Table 5). Nano-catalysts have made substantial advances in lignocellulosic biomass conversion. Lignocellulose, a complex plant cell wall structure, resists breakdown, making it a difficult bioenergy fuel. Nano-catalysts break down lignocellulosic materials more effectively than standard catalysts, minimizing high temperatures and chemical treatments.

* Table 5 can be found in the Appendix section.

Bioenergy processes are more selective and specific using nano-catalysts. They target particular reactions to reduce waste and byproducts. Selectivity is especially useful in bioenergy production, where biofuel purity and quality are crucial for performance and marketability, [41]. Nano-catalyst integration has also helped enzymatic catalysis. Nano-catalysts improve enzyme stability and reusability, boosting biomass breakdown and biofuel production. This interaction between nano-catalysts and enzymatic catalysis has enabled cost-effective and environmentally sustainable bioenergy conversion. Nano-catalysts are scalable, sustainable, and catalytic. They can accommodate different feedstocks and reactor designs due to their modest size and ease of integration into bioenergy operations. Nano-catalysts may also be synthesized sustainably, decreasing their environmental impact.

1.4 Nano-catalyst Essentials

Nano-catalysts, a cutting-edge technology, are essential in chemistry, materials science, and renewable energy. Nanoscale materials are changing catalysis and nanotechnology with their distinct features and capabilities. Catalysts of nanometer-scale dimensions have a high surface area-to-volume ratio, [42], [43], [44], [45]. This gives them many active areas for catalyzing chemical reactions, providing high efficiency and selectivity in many processes. They also accelerate chemical transformations due to their tiny size and increased dispersion and accessibility in reaction settings. Nano-catalysts' adaptability in many applications is a major benefit. Heterogeneous catalysis uses them immobilized on nanoparticles or surfaces, whereas homogeneous catalysis uses them completely distributed in solution, [46].

Nano-catalysis research continues to discover new catalyst materials, improve catalytic efficiency, and investigate nanomedicine and environmental remediation applications. Challenges such as catalyst stability, cost-effective manufacturing, and safety are still being studied, [47]. Understanding nano-catalysts is vital to recognizing their transformational potential in many scientific and commercial fields. As nanotechnology and catalysis research improves, nano-catalysts will push the limits of efficiency, sustainability, and innovation in chemistry and beyond.

1.5 Bioenergy Applications of Nano-catalysts

Nano-catalysts' catalytic characteristics make them appealing in bioenergy. These small yet powerful catalysts improve bioenergy conversion processes' efficiency, selectivity, and sustainability, helping produce cleaner, more sustainable energy sources, [48]. Lignocellulosic biomass conversion into biofuels is a major nano-catalyst bioenergy

application. Breaking down lignocellulosic biomass like cellulose and lignin into biofuels is difficult. With their high surface area-to-volume ratios and unique surface reactivity, nano-catalysts rapidly break down complex materials, [49], [50]. This increases bioethanol and biodiesel yields from lignocellulosic feedstocks without harsh chemical treatments or high temperatures.

Nano-catalysts improve enzyme stability and efficiency in enzymatic biofuel generation. Biocatalyst enzymes convert organic resources into biofuels. However, enzymes are susceptible to environmental conditions and are unstable.

1.6 Metal Oxide-based Nano-catalysts

In the field of bioenergy production, metal and metal oxide-based nanomaterials have garnered attention. Nano-catalysts such as metal oxides of alkali earth and transition metals have been found to be efficient, sustainable, and environmentally friendly for the production of biofuels like biodiesel. Nanotechnology presents a novel and practical approach to enhance the eco-friendly production of renewable biofuels, offering benefits such as enhanced catalytic efficiency and reduced environmental impact. Metallic, magnetic, and metal oxide nano-catalysts are employed as efficient biofuel additives. Some of the commonly used nano-catalysts, such as zirconium dioxide (ZrO_2), zinc oxide (ZnO), palladium (Pd), zero-valent iron (Fe^0), iron oxide, and TiO_2, have demonstrated their effectiveness in the production of biofuels from wastewater, providing enhanced yields and selectivity.

1.7 Synergy of Nano-catalysts and Enzymatic Catalysts

Magnetic nanoparticles (MNPs) have been extensively studied for their potential in bioenergy production due to some of the advantages, like high specific area, controllable particle size, and easy separation of these particles using an external magnetic field. Enzyme stability and reusability in biocatalytic reactions can be enhanced by using them as adaptable carriers for enzyme immobilization. Biodiesel, bioethanol, biohydrogen, and biogas are merely some of the biofuels that have been produced using MNPs. They increase the amount of biogas produced and its CH_4 content. MNPs boost bioethanol yields and enhance the enzymes' heat and storage stability during the bioethanol manufacturing process. Additionally, MNPs catalyze the synthesis of biodiesel, accelerating the process and promoting the immobilization of enzymes.

Integrating nano-catalysts with enzymatic catalysts is a potential catalysis frontier that uses nanotechnology and biotechnology to improve catalytic performance and extend reaction options. This synergy uses nano-catalysts' large surface area, customizable reactivity, and enzymatic catalysts' specificity and selectivity. These catalysts' collaboration potential and use in green chemistry and bioenergy production are examined in this study. Nano-catalysts, made of nanoparticles on the nanoscale scale, provide several catalytic benefits, [51]. Their high surface area-to-volume ratio affords many active sites for reactions, improving catalytic efficiency. Nano-catalysts may manipulate reaction pathways and selectivity by carefully engineering their catalytic characteristics. Enzymatic catalysts are known for their chemical selectivity. Biological catalysts can precisely conduct complex processes, surpassing conventional catalysts. They are interesting for different applications because of their moderate operation in ecologically acceptable aqueous solutions.

Microenvironment management has become an essential technique for catalytic reactions in chemistry and biology. This method optimizes catalyst performance, stability, and specificity by modifying local circumstances. Researchers can generate efficient and selective catalytic conditions by fine-tuning pH, temperature, and solvent characteristics, [52]. This study examines catalytic microenvironments' importance, methodologies, and uses, highlighting their vital role in many scientific and industrial endeavors. Enhanced catalysis by optimization of microenvironments, as mentioned in Table 6.

* Table 6 can be found in the Appendix section.

1.8 Maximizing Overall Bioenergy Efficiency

Sustainable and renewable energy sources need bioenergy efficiency optimization. From biomass conversion to biofuel production, bioenergy development requires efficiency advances at each step. Bioenergy efficiency may be improved by optimizing feedstock use. This comprises choosing and processing biomass resources with the best energy output per unit input, minimizing waste, and assuring sustainability, [53]. Advanced technologies like biorefineries can extract biofuels, chemicals, and minerals from biomass, increasing energy production.

Bioenergy conversion efficiency must also be improved. Advanced fermentation processes, enzyme optimization, and genetically engineered microbes may boost bioethanol output and minimize energy use. Innovations in anaerobic digestion systems and

co-digestion with organic waste streams may inspire biogas generation. Capturing and using bioenergy waste heat may boost efficiency, [54]. Nano-catalysts and enzymatic catalysts may also increase biochemical and biofuel production efficiency. Maximizing bioenergy efficiency needs feedstock selection, process optimization, and cutting-edge technology, making the bioenergy business more sustainable and profitable.

1.9 Real-world Applications and Case Studies

Real-world applications and case studies show how nano- and enzymatic catalysts aid numerous businesses and processes. A good example is biofuel production. Researchers have used bimetallic nanoparticles to catalyze biomass conversion into biofuels like biodiesel. Nano-catalysts boost yields and reaction kinetics by increasing surface area and catalytic activity. Enzymatic catalysts are crucial to biofuel production, especially in the hydrolysis of lignocellulosic biomass to bioethanol. Cellulases and xylanases effectively break down complex plant components into fermentable sugars, providing a sustainable bioenergy source, [55].

1.10 Addressing Wastewater Treatment Challenges

Maintaining environmental sustainability and public health requires addressing wastewater treatment issues. Nano-catalysts and enzymatic catalysts have revolutionized wastewater treatment by solving long-standing problems. Degrading organic wastewater pollutants is a significant use. Titanium dioxide nanoparticles may break down organic contaminants into harmless byproducts under UV or visible light. This photocatalytic method removes pharmaceutical residues and industrial pollutants from wastewater. The conventional techniques for wastewater treatment are shown in Table 7.

* Table 7 can be found in the Appendix section.

Wastewater treatment relies on enzymatic catalysts to degrade resistant chemicals. Dye and phenolic chemicals are broken down by peroxidases and laccases. These enzymes degrade target chemicals with remarkable selectivity and efficiency, removing hazardous contaminants from wastewater. Immobilization may also improve enzymatic catalyst stability and reusability in continuous treatment processes, lowering operating costs and environmental effects.

Nano-catalysts and enzymatic catalysts can also remove heavy metals from wastewater. Iron-based nanoparticles adsorb and reduce hazardous metal ions, making them less soluble and easier to precipitate or filter. Enzymatic catalysts like metalloenzymes may precipitate heavy metals, providing a greener alternative to chemical techniques. The use of these catalysts in wastewater treatment reduces pollution and supports resource recovery by reclaiming heavy metals. In conclusion, nano-catalysts and enzymatic catalysts may solve many of the problems in wastewater treatment. Their capacity to effectively digest organic pollutants, remove heavy metals, and recover resources makes them crucial to sustainable wastewater treatment.

1.11 Embarking on Sustainable Energy Initiatives

Sustainable energy efforts are essential to solving global energy problems and reducing climate change. Nano-catalysts and enzymatic catalysts in these efforts demonstrate a dedication to using modern technology for greener, more efficient energy generation. Nano-catalysts are essential in renewable energy. Nano-catalysts improve solar cell efficiency by absorbing light and transferring electrons, [56]. These catalysts boost solar panel energy conversion efficiency, decreasing fossil fuel use and carbon emissions.

In biofuel production, enzymatic catalysts have become popular in sustainable energy projects. Bioethanol and biodiesel are produced via enzymatic hydrolysis and transesterification of biomass feedstocks. Enzymatic catalysts convert complicated organic resources into more cost-effective and ecologically benign biofuels due to their selectivity. Enzymatic catalyst-driven biofuel generation from non-food feedstocks reduces food security and resource competitiveness problems. Nano-catalysts and enzymatic catalysts may expedite the shift to greener, more sustainable energy sources and lower their environmental impact.

Nano-catalysts and enzymatic catalysts also produce green chemicals and medications. Using precision and selectivity, enzymatic catalysts may efficiently produce complex medicinal compounds with less waste and environmental effects in pharmaceutical synthesis, [57]. Nano-catalysts have catalyzed chemical processes with excellent efficiency and selectivity, enabling green chemistry by synthesizing sustainable chemicals and materials. Numerous research studies have examined the topic of maximizing biodiesel production from waste cooking oil through the use of response surface methods and zinc-doped calcium oxide (Zn-doped CaO) based on lime. It has been investigated to create

effective and affordable catalysts from leftover egg shells using the wet impregnation method, [58].

According to research, a Zn-doped CaO nano-catalysts exhibits great promise for producing biodiesel, with maximum conversion rates of 96.74% attained under ideal circumstances, [59]. The impacts of key operating factors on biodiesel yield, such as catalyst concentration, reaction temperature, and the methanol-to-oil molar ratio, were examined in another study. The most crucial factor was discovered to be the catalyst concentration, and a maximum biodiesel output of 99.38% was attained, [60].

1.12 Industry Implications

Nano-catalysts and enzymatic catalysts may revolutionize many sectors' processes, products, and environmental stewardship. Nano-catalysts will transform renewable energy. Photovoltaic cells, catalytic converters, and fuel cells may improve energy conversion efficiency and minimize greenhouse gas emissions with their utilization, [61]. These catalysts promise cleaner, more sustainable power production by effectively harvesting solar and H_2 energy, which is crucial for climate change and energy security.

The chemical and pharmaceutical sectors profit greatly from enzymatic catalysts. These catalysts produce high-value chemicals and medicines with unmatched accuracy and selectivity. Green chemistry reduces these sectors' environmental impact by synthesizing complex compounds efficiently and with little waste. Enzymatic catalysts can also manufacture bio-based chemicals and medicines, helping to transition away from petrochemicals and towards a circular economy.

1.13 Future Research Avenues

Nano-catalyst and enzymatic catalyst research will affect sustainability, innovation, and environmental stewardship. Multi-functional catalysts that execute many reactions in one catalytic system are promising, [62]. Researchers may simplify processes, minimize resource consumption, and improve chemical transformation efficiency by creating catalysts with many active sites or enzymatic and nano-catalytic components. These multifunctional catalysts might revolutionize the chemical industry and environmental remediation, where complicated reactions need numerous stages and reagents.

Catalyst design research on sustainable materials is projected to increase. This involves developing catalysts from renewable and biodegradable materials and adding waste-derived components to reduce environmental effects. Future research may use green chemistry to create little waste, energy, and synthesis catalysts. Additionally, studying catalytic techniques that employ non-toxic solvents or mild conditions might help lessen the environmental impact of catalyst manufacture and use, [63]. Nano-catalyst and enzymatic catalyst research might improve catalysis in several disciplines and businesses by making it more sustainable, efficient, and environmentally friendly.

Silicon dioxide, (also known as silica or SiO_2), is an oxide of silicon, commonly found in nature as quartz, [64]. In many parts of the world, silica is the major constituent of sand, [65]. Silica is one of the most complex and abundant families of materials, existing as a compound of several minerals and as a synthetic product, [65]. For instances, include fused quartz, fumed silica, opal, and aerogels. SiO_2 is used as a component in structural materials, microelectronics, food, and pharmaceutical industries, [66]. All forms of SiO_2 are white or colorless; however, impure samples may be colored. SiO_2 is a common fundamental constituent of glass, [66].

SiO_2 is especially appealing because of its anticidal characteristics, which may kill bacteria, molds, viruses, and even cancer cells, [67], [68]. SiO_2 has no photocatalytic activity, which is a significant issue. Researchers have sought to build a visible-light SiO_2 based photocatalyst and an antibacterial agent to address these issues. There are three basic methods for preparing such agents: (1) noble metal ion or transition metal ion doping such as platinum (Pt), gold (Au), silver (Ag), vanadium (V), chromium (Cr), manganese (Mn), iron (Fe), cobalt (Co), and nickel (Ni); (2) N_2 doping; and (3) coupling with a small-band gap semiconductor that extends light absorption into the visible region. Metal doping (particularly Ni and Co) has received a lot of attention among these alternatives. Ni and Co are thought to improve photocatalytic activity by facilitating electron−hole separation and/or providing more adsorption surface area. It is thought that visible light absorption by Ni and Co surface plasmons induces electron transfer to Fe_2O_3, resulting in charge separation and thus activation by visible light, [68], [69], [70], [71].

Iron (III) oxide, [also known as ferric oxide, α-iron (III) oxide (α-Fe_2O_3), Fe_2O_3 or hematite], is the inorganic compound, [72]. It occurs in nature as the mineral hematite, and is the main source of iron for the steel industry, [72]. It is also known as red iron oxide, especially when used in pigments, [72].

The Fe_2O_3 is a more attractive alternative adsorbent for water treatment as it is cost-effective and non-toxic. The physicochemical properties of the Fe_2O_3/SiO_2 MNCs are superior and can be used as

adsorbents for a wide variety of reactions, [73], [74], [75]. The comparison of Fe_2O_3/SiO_2 MNCs applications for different literature studies were evaluated at Table 8.

* Table 8 can be found in the Appendix section.

GOx is used in a variety of industries, including food, beverage, textiles, clinical research, and biotechnology, [76], [77]. Baking, dairy products, starch conversion, and beverage processing (beer, wine, fruit, and vegetable juices) are various applications of the GOx enzyme in the food industry, [78]. The use of GOx enzyme in increasingly advanced sectors such as biosensors, is fast growing due to the specificity of enzymes, which is of a key position in biosensors, [79], [80], [81]. They are used to detect, transmit, and record data that is then processed into an analytical signal, allowing them to be employed in a variety of applications, [79], [82], [83]. Many other key sectors, such as health care, pharmaceuticals, and chemical manufacturing, are taking advantage of GOx's remarkable properties, [84], [85]. Carbon felt, Au nano-stars, cellulose nanocrystals, carbon nanotubes (CNTs), nanofibers, and other materials have been used to immobilize GOx due to its industrial value, [86], [87], [88]. Although, among the various supports, magnetic supports for biological and biomedical materials are of specific attention due to their intrinsic characteristics, such as non-toxicity, large surface area, and capacity to generate required magnetic properties, as well as their capability to be separated with magnets and be recycled, [88], [89]. Immobilization of enzymes, however, has several drawbacks, including inadequate immobilization, mass transfer, and diffusion limitation. The surface chemical characteristic of the support material, i.e., functional groups present on the surface, has a significant impact on the performance of immobilized enzymes. The presence of valuable functional groups on the surface can help enzymes integrate better, resulting in more active enzyme loading and less leaching during applications, [90].

2 Material and Methods

2.1 Chemicals

SiO_2 or Silica was purchased from Sigma-Aldrich (Merck). Iron (III) oxide (Fe_2O_3) > 99.00% was obtained from Sigma-Aldrich (Merck). Glucose oxidase (GOx) enzymatic nano-catalysts isolated from *Aspergillus niger* were purchased from E. Merck (Germany) and Sigma Aldrich (St. Louis, MO, USA).

All reagents or chemicals used were of analytical grade (95% to 99%, purity grade). Iron nitrate nonahydrate [$Fe(NO_3)_3.9H_2O$], nickel nitrate hexahydrate [$Ni(NO_3)_2.6H_2O$], cobalt nitrate hexahydrate [$Co(NO_3)_2.6H_2O$], tetraethoxysilane (TEOS), sodium hydroxide (NaOH), sodium chloride (NaCl), glycine ($C_2H_5NO_2$), sodium acetate (CH_3COONa), sodium phosphate (Na_3PO_4), ethanol (EtOH), hydrochloric acid (HCl), 3-aminopropyl triethoxysilane (APTES), dimethylformamide (DMF), 2-hydroxy-3,5-dinitrobenzoic acid (DNSA), glutaral dehyde (GA), and glucose oxidase (GOx) isolated from *Aspergillus niger* were procured from E. Merck (Germany) and Sigma Aldrich (St. Louis, MO, USA).

2.2 GOx Enzymatic Nano-Catalysts

The glucose oxidase enzyme (GOx or GOD) also known as notation (EC number 1.1.3.4) is an oxidoreductase that catalysis the oxidation of glucose to hydrogen peroxide (H_2O_2) and D-glucono-δ-lactone. This enzyme is produced by certain species of fungi and insects and displays antibacterial activity when O_2 and glucose are present, [91].

GOx is widely used for the determination of free glucose in body fluids (medical testing), in vegetal raw material, and in the food industry, [92]. It also has many applications in biotechnologies, typically enzyme assays for biochemistry including biosensors in nanotechnologies, [50], [77].

2.3 GOx Enzymatic Nano-Catalysts coated with Fe_2O_3/SiO_2 MNCs

2.3.1 Chemicals for GOx Enzymatic Nano-Catalysts

Iron nitrate nonahydrate ($Fe(NO_3)_3.9H_2O$), tetraethyl orthosilicate (or tetra ethoxy silane, TEOS), sodium hydroxide (NaOH), sodium chloride (NaCl), glycine ($C_2H_5NO_2$), sodium acetate (CH_3COONa), sodium phosphate (Na_3PO_4), ethanol (EtOH), hydrochloric acid (HCl), 3-aminopropyl tri ethoxy silane (APTES), dimethylformamide (DMF), 2-hydroxy-3,5-dinitrobenzoic acid (DNSA), glutaraldehyde (GA), and GOx isolated from *Aspergillus niger* were procured from E. Merck (Germany) and Sigma Aldrich (St. Louis, MO, USA).

2.4 Preparation of Ferrite (Fe_2O_3) NCs Coated with Silica (Fe_2O_3/SiO_2 MNCs)

The sol-gel auto-combustion method was used to make nanocrystalline Fe_2O_3–coated-SiO_2 MNCs. The sol−gel auto-combustion method was described by

Nasir et al., [8]. The molar ratio was fixed at 1/4/7 (TEOS/EtOH/H_2O), and TEOS diluted in EtOH was slowly added into deionized water. To maintain an acidic pH=2.0, an appropriate amount of acetic acid was added to the solution. When the precursor solution was stirred at 50°C for 2 h, TEOS hydrolysis occurred, yielding a transparent viscous solution (Solution A, Sol A).

$Fe(NO_3)_3$, and citric acid were dissolved in deionized water to make Solution B (Sol B). The citric acid to metal ions molar ratio was fixed at 1:1. To adjust the pH=7.0, an appropriate amount of ammonia (NH_3) was added to the solution. After that, Sol A and Sol B was mixed to form a homogeneous transparent aqueous solution. The solution was evaporated at around 70°C until a transparent sol was obtained, and then the resultant sol was heated at 110°C for 24 h to allow the dried gel formation. When the dried gel was ignited in the air at 250°C, it self-propagated. The as-burnt Fe_2O_3/SiO_2 MNCs were reddish-brown and voluminous.

2.5 GOx Immobilization on Fe_2O_3 NCs Coated with SiO_2 NCs Activation of MNCs

To activate Fe_2O_3/SiO_2 MNCs, they are first salinized with 3-aminopropyl tri ethoxy silane (APTES) and then activated with the coupling agent glutaraldehyde (or D-gluconic acid, GA). For salinization, 30 mg of each series of Fe_2O_3/SiO_2 MNCs were ultrasonically dispersed in 5 ml of 70% EtOH solution for 30 min, and then equal volumes of APTES and dimethylformamide (DMF) (0.25 ml each) were added to the dispersed nanocomposite solution. The solutions were stirred for 4 h at 300 rpm, and then salinized nanocomposites were collected by applying a small magnetic field to them. To get GA activated nanocomposites, 10 ml (2 mg/ml) of salinized nanocomposites were dispersed into 10 mM Phosphate buffered saline (PBS) (pH=7.3), then 400 µl of 0.5% GA solution was added to the dispersed solution, and the entire reaction mixture was kept stirring (300 rpm) at 30°C for 1 h and lastly washed several times with PBS. The activated carriers are redispersed in the 5 ml of PBS to be used again.

2.6 GOx Immobilization with Activated Fe_2O_3 NCs-Coated SiO_2 NCs

For the immobilization of GOx, activated Fe_2O_3/SiO_2 MNCs were resuspended into 100 mM phosphate buffer solution of pH=6.0 to make a final concentration of 3 mg/ml and then 4 mg of GOx was mixed with 6 ml of resuspended nano-ferrite composites and kept stirring for 2 h at 4°CC. After stirring, the reaction mixture was washed several times with the same buffer and the whole solution was placed under the influence of a permanent magnet to remove the unbound GOx. Finally, stock solutions of immobilized GOx on Fe_2O_3/SiO_2 MNCs were stored at 4°C until used.

2.7 Adsorption Mechanisms with the Sol−Gel Auto-Combustion Method

Properties of immobilized GOx and loading efficiency of GOx to test the industrial applicability of Fe_2O_3/SiO_2 NCs**.** GOx was covalently immobilized on the surface of Fe_2O_3/SiO_2 via gluconic acid (GA), which acted as a linker between GOx and nanocomposites, [93] (Fig. 5). The loading efficiency of GOx was 85% on the GA activated surface of Fe_2O_3/SiO_2 NCs.

* Figure 5 can be found in the Appendix section.

GOx is an oxidoreductase that catalyses the oxidation of β-D-glucose to D-glucono-δ-lactone with molecular O_2, and the intermediate lactone extemporaneously hydrolyses into GA and H_2O_2 by lowering the reaction's activation energy, [42], and this reaction was shown as following figure (Fig. 5).

The sol–gel auto-combustion technique is primarily used to synthesize nanosized oxides via an exothermic reaction between oxidants (typically metal nitrates) and fuel (such as organic amines, urea and acids, [94]. the combustion process, gases such as CO_2, nitrogen dioxide (NO_2), and nitrogen oxide (NO) are released, and the metal oxides will be formed simultaneously through the decomposition of the nitrates. Meanwhile, reduction gases such as H_2, CH_4, and NH_3 are released as well and play an important role in the reduction of the metal oxides according to a previous study, [95]. The combustion reaction can be simply described as follows (where M denotes the metal atom/ ions and n is the metal valence) equations are Eq. (3), Eq. (4), Eq. (5) and Eq. (6):

$$2NH_4NO_3 \rightarrow 2NH_3\uparrow + NO_2\uparrow + NO\uparrow + H_2O\uparrow + O_2\uparrow \quad (3)$$

$$C_6H_8O_7 + H_2O \rightarrow 4CO_2\uparrow + 2CH_4\uparrow + H_2\uparrow \quad (4)$$

$$M(NO_3)_n + C_6H_8O_7 + \left(\frac{5n}{2} + 7\right)O_2 \rightarrow \frac{1}{2}M_2O_n + 6CO_2\uparrow + 4H_2O\uparrow + \frac{n}{2}N_2\uparrow \quad (5)$$

$$5M_2O_n + nH_2 + nCH_4 \rightarrow 10M + 3nH_2O + nCO_2 \quad (6)$$

Thermogravimetric–differential scanning calorimetry–mass spectrometry (TG–DSC–MS) analysis was performed to analyse the combustion reaction, and the gas composition of the dried gel with a fuel-oxidant ratio of 1/1. The TG–DSC–MS results show that the gas phases play an important role in the mechanism behind the sol-gel auto-combustion process. Different fuel-oxidant ratios will promote the formation of different gas components, which will significantly affect the composition and structure of the final product. To optimize the fuel–oxidant ratio, reagents with different fuel-oxidant ratios (0.8/1, 0.9/1, 1/1, 1.1/1, and 1.2/1) were dissolved in deionized water to obtain the sols. The dried gels were then activated by combustion at a temperature of 300°C based on the TG–DSC–MS results.

As a result, the Co^{2+}, Cr^{3+}, Cu^{2+}, Ni^{2+}, and Al^{3+} ions will be homogeneously distributed in the dried gels, and no interface will exist between the metal ions. Compared to traditional HEAs synthesis techniques requiring long periods of time for the diffusion of the atoms to form solid solutions, the in situ chemical reactions described in Eq. (3) groups (4) only require a short-range diffusion of the atoms to form solid solutions.

According to Boltzmann's hypothesis regarding the relationship between the entropy of a system and the system complexity, for a random solid solution, the configurational entropy of mixing is represented by the following Eq. (7):

$$\Delta S_{mix} = -R\sum_i c_i ln c_i \quad (7)$$

where R is the gas constant (8.314 J/K mol) and c_i is the molar content of the i^{th} component, [96]. Thus, for an equiatomic alloy with n components, the configurational entropy of mixing is Eq. (8):

$$\Delta S_{mix} = Rlnn \quad (8)$$

For an Equi atomic alloy with 3, 4, and 5 principal components, ΔS_{mix} is 1.10*R*, 1.39*R*, and 1.61*R*, respectively. In fact, complex phases or inter metallics easily form in alloy systems with multiple principal components according to traditional metallurgical knowledge, [97], and simple solid solutions will be formed when the alloys contain more than five principal elements because of the high mixing entropy (> 1.61*R*) according to the knowledge about high-entropy alloys (HEAs). However, CoCuNi (ternary, ΔS_{mix}=1.10*R*) and CoCrCuNi (quaternary, ΔS_{mix}=1.39*R*) Equi atomic solid solution alloys without a high mixing entropy were synthesized in this study. Therefore, according to the above discussion, some Equi atomic solid solution alloys can be synthesized eluding the restriction of a high mixing entropy, which further indicates the superiority of the sol–gel auto-combustion technique for the preparations of solid solution HEAs.

The HEA powder prepared via MA showed a ferromagnetic behaviour, and the saturated magnetizations (M_S), remanence ratio (M_R/M_S) and coercivity force (H_C) were measured to be 2.521 emu/g, 17.30%, and 238.867 Oe, respectively. However, compared to the magnetic properties of the CoCrCuNiAl HEA synthesized via MA, the corresponding HEA synthesized via the sol–gel auto-combustion showed a distinctive soft magnetic behaviour and higher saturated magnetizations (13.372 emu/g), a lower remanence ratio (1.93%), and a lower coercivity force (10.528 Oe). Furthermore, the HEA powder synthesized via the sol–gel auto-combustion showed a behaviour similar to a superparamagnetic behaviour because of the low remanence ratio. In general, magnetic nanoparticles with diameters < 10 nm exhibited a superparamagnetic behaviour, [98]. The CoCrCuNiAl HEA synthesized via the sol-gel auto-combustion had an average grain size of 14 nm, and can easily lead to the observed magnetic behaviour similar to a superparamagnetic behaviour. This makes HEAs prepared via the sol-gel auto-combustion promising candidates for future applications in some special conditions.

Combining the sol-gel and auto-combustion methods results in a simple and inexpensive preparation method for high purity, homogenous nano-powder at low annealing temperature, [99], [100]. The method consists in dissolving nitrate salts in water, addition of the organic complexing agent (citric acid), adjustment of the solution to pH=7.0, heating at 70ºC to form the sol, and then at 110ºC to remove the residual water and form the gel, and initiation of the autocatalytic self-combustion process of nitrate-fuel gel, [101]. The citric acid and glucose are two of the most used fuels due to their strong complexing ability and low ignification temperature (200–250ºC), [101]. The synthesis of $CoFe_2O_4$ nanoparticles (NPs) in the size range of 11–40 nm by the sol-gel auto-combustion method and annealing at different temperatures (800–1000ºC) was also reported, [101].

2.8 Photocatalytic Degradation Measurements

Under UV light irradiation against samples, the photocatalytic activity of nano crystalline Fe_2O_3 (x = 0.5, 1.0) / SiO_2 MNCs was measured. A total of 30 µg/ml of each Fe_2O_3/SiO_2 MNCs was added to 100 ml

GOx enzymatic nano-catalysts solution (25 μg/ml) in the photocatalytic degradation experiment. Before irradiation, the suspensions containing samples and Fe_2O_3 (x = 0.5, 1.0)/SiO_2 MNCs were magnetically stirred in the dark for 120 min to ensure the establishment of an adsorption/desorption equilibrium, respectively. Aliquots (5 ml) were sampled at a fixed time interval (up to 120 min) and then magnetically separated to remove essentially all of the Fe_2O_3 (x = 0.5, 1.0) / SiO_2 MNCs. A UV−vis spectrophotometer (Perkin Elmer Life and Analytical Sciences, CT, USA) was used to record variations in the maximum absorption band (A_{668} nm) of the filtrate in the wavelength range of $A_{200–800}$ nm. The following formula was used to calculate the photocatalytic degradation of the samples via the photocatalytic activity of Fe_2O_3/SiO_2 MNCs at Eq. (9):

$$Photocatalytic\ Degradation\ (\%) = \frac{C_0 - C}{C_0} \qquad (9)$$

where C_0 represents the initial concentration of the samples before photodegradation and C represents the absorbance at various time intervals.

2.9 Analytical Methods

All experimental analysis were determined with Standard Methods, [102].

2.10 GOx Enzymatic Nano-Catalysts Analyses

2.10.1 Standard Activity Assay of GOx Enzymatic Nano-Catalysts

The catalytic activities of both soluble and immobilized GOx enzymatic nano-catalysts were analysed by a UV-vis spectrophotometer using DNSA as a chromogenic substrate, [83]. The standard reaction mixture in a total volume of 2 ml contained 8 μg of GOx enzymatic nano-catalysts and 5 mM glucose in 100 mM phosphate buffer, pH=6.0. The reaction was initiated by the addition of glucose, followed by incubation at room temperature with continuous stirring for 10 min. After incubation, the reaction was stopped by the addition of 2 ml DNSA solution and then the whole solution was boiled for 10 min at 100°C, a bright orange colour appeared and finally absorbance was measured at 576 nm. Appropriate reaction blanks were used for both the soluble and immobilized GOx enzymatic nano-catalysts, i.e., for the soluble enzyme, all components of the reaction mixture were present in the blank except the enzyme, and for the immobilized enzyme, all components of the reaction mixture including Fe_2O_3/SiO_2 MNCs were present in the blank except the immobilized enzyme.

2.10.2 Optimization of pH and Temperature for Immobilized GOx Enzymatic Nano-Catalysts

The optimization of pH for the enzymatic activities of soluble and immobilized GOx enzymatic nano-catalysts was performed in 100 mM of different buffers of pH ranging from 3.0 to 10.0. The buffers used were glycine-HCl (pH=3.0), sodium acetate (pH=5.0), sodium phosphate (pH=6.0, pH=7.0), and Tris−HCl (pH=8.0−10.0). For calculating the percent residual catalytic activity at different pH ranges, the catalytic activity at pH=5.5 and pH=6.0 was chosen as the maximum activity (100%) for the soluble and immobilized GOx enzymatic nano-catalysts, respectively. The optimization of temperature for catalytic activities for soluble and immobilized GOx enzymatic nano-catalysts was performed under standard reaction conditions in 100 mM of sodium phosphate buffer of pH=6.0 by varying temperatures ranging from 25−65°C. For calculating the residual percent catalytic activity at different temperatures, the activities at 40 and 45°C were chosen as the 100% maximum residual activity for soluble and immobilized GOx enzymatic nano-catalysts, respectively. All the assays were performed in triplicates, and results were reported as a mean value.

2.10.3 The Determination of Kinetic Constants

For the kinetic constants determination was used varying concentrations of glucose (10−150 mM) as a substrate in 100 mM PBS buffer of pH=6.0 at standard reaction conditions to determine kinetic parameters such as the maximum velocity (V_{max}) and Michaelis−Menten constant (K_m) of soluble and immobilized GOx enzymatic nano-catalysts. The apparent values of V_{max} and K_m of both the formulations were calculated by using the Lineweaver Burk plot (double reciprocal plot).

2.10.4 Determination of GOx Enzymatic Nano-Catalysts Loading Efficiency.

The loading efficiency of GOx enzymatic nano-catalysts on the Fe_2O_3/SiO_2 MNCs was calculated by using the following equation, [90], in Eq. (10):

$$Loading\ Efficiency\ (\%) = \frac{C_0\,V_0 - C_i\,V_i}{C_0\,V_0}\ x\ 100\% \qquad (10)$$

where C_0 represents the initial concentration of GOx stock and V_0 represents the volume of the GOx solution prior to immobilization. C_i stands for the concentration of GOx in washed fraction, and V_i stands for the volume of the filtrate, which was left after immobilization.

2.10.5 Reusability Analysis

To explore the reusability and recovery of immobilized GOx enzymatic nano-catalysts from the reaction mixture, we assessed the activity of immobilized GOx enzymatic nano-catalysts for repetitive cycles. After each repetitive cycle, immobilized GOx enzymatic nano-catalysts was washed 2−3 times with assay buffer and recovered from the solution by centrifugation at 4000 rpm for 20 min, respectively. After centrifugation, the supernatant was discarded and the pellet was resuspended in the activity buffer and stored at 4°C for another cycle, so these procedures were recurring for 10 days cycles in a row. The activity of immobilized GOx enzymatic nano-catalysts determined on the first day is considered as the 100% maximum residual activity for the evaluation of the remaining percent residual activity after repetitive cycles.

2.11 Characterisations

2.11.1 X-Ray Diffraction (XRD) Analysis

Powder XRD patterns were recorded on a Shimadzu XRD-7000, Japan diffractometer using Cu Kα radiation (λ = 1.5418 Å, 40 kV, 40 mA) at a scanning speed of 1° /min in the 10-80° 2θ range. Raman spectrum was collected with a Horiba Jobin Yvon-Labram HR UV-Visible NIR (200-1600 nm) Raman microscope spectrometer, using a laser with the wavelength of 512 nm. The Raman spectrum was collected from 10 scans at a resolution of 2 /cm. The zeta potential was measured with a SurPASS Electrokinetic Analyzer (Austria) with a clamping cell at 300 mbar.

2.11.2 Fourier Transform Infrared Spectroscopy (FTIR) Analysis

The FTIR spectra of samples was recorded using the FT-NIR spectroscope (RAYLEIGH, WQF-510). Experimental Fe_2O_3/SiO_2 MNCs samples were scanned using infrared light and their chemical properties were obtained in FTIR spectra.

2.11.3 Field Emission Scanning Electron Microscope (FESEM) Analysis

The morphological features and structure of the synthesized catalyst were investigated by SEM (FESEM, Hitachi S-4700). To investigate the composition of the elements, present in the synthesized Fe_2O_3/SiO_2 magnetic nanocomposites; SEM images were used.

2.11.4. Energy Dispersive X-Ray (EDX) Analysis

To investigate the morphological properties and structure of the synthesized catalyst and the composition of the elements present in the synthesized catalyst; an EDS spectrometry instrument (TESCAN Co., Model III MIRA) was used.

2.11.5 UV-vis Spectroscopy Analysis

A UV−vis spectrophotometer (Perkin Elmer Life and Analytical Sciences, CT, USA) was used to record variations in the maximum absorption band (A_{668} nm) of the filtrate in the wavelength range of $A_{200–800}$ nm. UV-visible spectra of samples were recorded from 200 to 400 nm in the presence and absence of Fe_2O_3/SiO_2 MNCs. Throughout, the experiment, a consistent concentration of samples (40 μM) was subjected to titration with diverse concentrations (ranging from 2.38×10^{-5}–3.19×10^{-4} g/ml) of Fe_2O_3/SiO_2 MNCs. Baseline correction was performed using a Tris-HCl buffer to ensure accurate readings and account for any background variations. The purpose of these measurements Fe_2O_3/SiO_2 MNCs at different concentrations (5, 10, 15, 20 and 25 mg/l).

2.11.6 High Resolution Transmission Electron Microscopy (HRTEM) Analysis

The size and structure of the Fe_2O_3/SiO_2 MNCs samples were identified with TEM analysis. The obtained Fe_2O_3/SiO_2 MNCs was collected and harvested by centrifugation (8000 rpm, 5 min), washed twice with deionized water and resuspended in ethanol (C_2H_6O) and dripped onto a carbon-coated copper (C-Cu) TEM grid. Vacuum drying then occurred to the Fe_2O_3/SiO_2 MNCs for 24 h at 25°C room temperature. The dry samples on the Cu grid were viewed and examined by TEM analysis recorded in a JEOL JEM 2100F, Japan under 200 kV accelerating voltage.

2.11.7 Vibrating-Sample Magnetometer (VSM) Analysis

Vibrating Sample Magnetometers (VSM) are cutting-edge instruments that play a vital role in studying and characterizing magnetic materials. The "vibrating" aspect of VSM is the key to its sensitivity and accuracy. When a sample vibrates within the magnetic field, any alterations in its magnetic characteristics result in measurable changes in the induced voltage. This voltage, known as the magnetization signal, is carefully recorded, enabling researchers to create detailed magnetization curves and analyze magnetic properties such as magnetic moment, coercivity, and remanence. In order to explain the magnetic property of Fe_2O_3/SiO_2 MNCs, the magnetic hysteresis curve was measured at 25°C.

The hysteresis loop exhibits ferromagnetic behavior with saturation magnetization (Ms) of 32.88 emu/g.

The experimental magnetic Fe_2O_3/SiO_2 MNCs samples for magnetic prooerties, vibrating, sensivity and accuracy measurements analyzed by gas chromatography–mass spectrometry (GC-MS) and gas chromatograph (GC) (Agilent Technology model 6890N) equipped with a mass selective detector (Agilent 5973 inert MSD) (as a kind of VSM instrument). Mass spectra were recorded using a VGTS 250 spectrometer equipped with a capillary SE 52 column (HP5-MS 30 m, 0.25 mm ID, 0.25 μm) at 220°C with an isothermal program for 10 min. The initial oven temperature was kept at 50°C for 1 min, then raised to 220°C at 25°C/min and from 200 to 300°C at 8°C/min, and was then maintained for 5.5 min. High purity helium gas [He(g)] was used as the carrier gas at constant flow mode (1.5 ml/min, 45 cm/s linear velocity).

2.12 Statistical Analysis

ANOVA analysis of variance between experimental data was performed to detect F and *P* values. The ANOVA test was used to test the differences between dependent and independent groups, [103]. Comparison between the actual variation of the experimental data averages and standard deviation is expressed in terms of F ratio. F is equal (found variation of the date averages/expected variation of the date averages). *P* reports the significance level, and d.f indicates the number of degrees of freedom. Regression analysis was applied to the experimental data in order to determine the regression coefficient R^2, [104]. The aforementioned test was performed using Microsoft Excel Program.

All experiments were carried out three times and the results are given as the means of triplicate samplings. The data relevant to the individual pollutant parameters are given as the mean with standard deviation (SD) values.

3 Results and Discussions

3.1 XRD Analysis Results

XRD patterns were determined for SiO_2 NCs (Fig. 6a), Fe_2O_3 NCs (Fig. 6b), Fe_2O_3/SiO_2 MNCs before photocatalytic degradation process (Fig. 6c), and GOx enzymatic nano-catalysts on coated with Fe_2O_3/SiO_2 MNCs after photocatalytic degradation process (Fig. 6d), respectively.

* Figure 6 can be found in the Appendix section.

Fig. 6a shows the amorphous state of SiO_2 NCs with a broad peak at 2θ angles 15.00° and 40.00°. Fig. 6b shows crystalline peaks for Fe_2O_3 NCs appeared at 2θ angles of 43.4°, 49.22°, 53.5°, 57.40° and 74.6°. The composite material Fe_2O_3/SiO_2 MNCs at Fig. 6c had crystalline structure at 2θ values 35.3°, 44.73°, 56.1° and 63.8° corresponding to Fe_2O_3 NCs. The broad peak at 2θ 15.0° and 30.0° (Fig. 6c) indicates the presence of SiO_2 NCs.

Fig. 6d shows XRD patterns for GOx enzymatic nano-catalysts on coated with Fe_2O_3/SiO_2 (x = 0.5, 1.0) MNCs after photocatalytic degradation process. A hump around $2\theta \approx 23°$ can be seen in all of the spectra, which corresponds to the amorphous matrix of SiO_2. The powder samples of GOx enzymatic nano-catalysts on coated with Fe_2O_3/SiO_2 MNCs show diffraction peaks at $2\theta \approx 30.10^o$ (220), 35.57^o (311), 43.16^o (400), 54.10^o (511), and 62.51^o (440), which could be easily indexed to the face-centered cubic (FCC) spinel structure of Si-O ferrite by comparing with JCPDS File No. 03-0864 (Fig. 6).

The discrepancy in FWHM is in agreement with the crystallite size calculated by Debye−Scherrer's formula as follow in Eq. (11), [105]:

$$D = \frac{0.9\,\lambda}{\beta \cos\theta} \tag{11}$$

Where, λ is the wavelength of Cu Kα radiation, D is the particle size, β is the full width half maximum intensity, and θ is the position of the peak. The main diffraction peak (311) was used to calculate the crystallite size = 17.37 nm from 2θ = 35.57 and FWHM (β) = 0.48 values, respectively.

3.2 FTIR Analysis Results

The FTIR spectra are shown in Fig. 7, aided in determining the pattern of the spinel structure in Fe_2O_3/SiO_2 MNCs. Pure GOx enzymatic nano-catalysts spectra was shown at Fig. 7a.

* Figure 7 can be found in the Appendix section.

In addition to, immobilized Fe_2O_3 NCs coated with SiO_2 NCs was determined with FTIR spectra at Fig. 7b. Strong absorption bands were observed in the prepared sample at 467, 799, 1090, and 1631 cm^{-1}, which can be attributed to Si−O−Si symmetric bond stretching vibrations, vibration mode of the ring structure of SiO_2 tetrahedra, [106], [107], Si−O−Si asymmetric bond stretching vibrations, [79], and bending vibrations of H−O−H absorbed in silica, [108], [109], [110], [111], [112], respectively. The generation of a silica network is shown by the typical absorption bands at 1090, 799, and 467 cm^{-1}, [63],

[113], [114]. The shoulder at 954 cm^{-1} was most likely attributable to Si−O−Fe vibrations as well Si−O−H stretching vibrations, [87], [115], [116], [117]. The occurrence of Si−O−Fe vibrations indicated some interactions between the Fe^{3+} ions and the surrounding silica network.

3.3 FESEM Analysis Results

FESEM analysis was applied to the synthesized Fe_2O_3/SiO_2 MNCs after experimental studies (Fig. 8). FESEM images were shown for Fe_2O_3 NCss (Fig. 8a), SiO_2 NCs (Fig. 8b), Fe_2O_3/SiO_2 MNCs (before photocatalytic degradation process) (Fig. 8c), and Fe_2O_3/SiO_2 MNCs (after photocatalytic degradation process) (Fig. 8d), respectively, with FESEM images size: 20 μm.

* Figure 8 can be found in the Appendix section.

At Fig. 8d illustrates the morphology of the synthesized Fe_2O_3/SiO_2 MNCs after photocatalytic degradation process showing spherical particles with an average size of approximately 39 nm.

3.4 EDX Analysis Results

The EDX spectrum of Fe_2O_3/SiO_2 MNCs (Fig. 9) confirms the presence of Fe, Si, C, N, and O elements, with atomic percentages of 15.60%, 12.41%, 22.64%, 2.95%, and 46.40%, respectively. EDX images were determined for SiO_2 NCs (Fig. 9a) Fe_2O_3 NCs (Fig. 9b), Fe_2O_3/SiO_2 MNCs before photocatalytic degradation process (Fig. 9c), and Fe_2O_3/SiO_2 MNCs after photocatalytic degradation process (Fig. 9d), respectively.

* Figure 9 can be found in the Appendix section.

The prepared SiO_2 NCs material (Fig. 9a) shows the weight percentage of 78.50% Si and 21.50% O. Fig. 9b shows that the Fe_2O_3 NCs material was composed of O, Fe and C, respectively, with the weight percentage given as 36.70%, 34.50% and 28.80%, respectively. The EDS peaks on Fe_2O_3/SiO_2 MNCs demonstrate confirmed the presence of Fe, Si, O and C, and the carbon peak that can be observed from EDS spectrum (Fig. 9a and 9b) originated from the carbon coating. The presence of Si indicates the formation of a SiO_2 shell using TEOS, [71], [118] while Fe and O correspond to the Fe_2O_3 NCs core. The strong bands of N and C suggest successful loading of PNV onto the surface of Fe_2O_3/SiO_2 MNCs, [86], [119], [120].

3.5 UV-vis Spectroscopy Analysis Results

A UV−vis spectrophotometer (Perkin Elmer Life and Analytical Sciences, CT, USA) was used to record variations in the maximum absorption band (A_{668} nm) of the filtrate in the wavelength range of $A_{200-800}$ nm. UV-vis spectra of samples were recorded from 200 to 800 nm wavelengths in the presence of Fe_2O_3/SiO_2 MNCs (Fig. 10). The absorbance values of Fe_2O_3/SiO_2 MNCs were ranged between 0.9 and 1.3

* Figure 10 can be found in the Appendix section.

3.6 HRTEM Analysis Results

HRTEM images of Fe_2O_3/SiO_2 MNCs were shown for before photocatalytic degradation process (Fig. 11a), without immobilized GOx enzymatic nano-catalysts (Fig. 11b), and at Fig. 11c with immobilized GOx enzymatic nano-catalysts, respectively. and HRTEM image size: 100 nm.

* Figure 11 can be found in the Appendix section.

HRTEM images of Fe_2O_3/SiO_2 MNCs without (Fig. 11b) and with (Fig. 11c) immobilized GOx enzymes are shown with their size distributions. Un-immobilized nanocomposites appeared to be very well and uniformly dispersed, with diameters ranging from 20 to 30 nm and an overall mean diameter of 22.90 ± 7.11 nm. However, after immobilization, the nanocomposites stay isolated and have a mean diameter of 20.65 ± 5.46 nm, which is similar to that of un-immobilized ones. The discrepancy in size between bare nanocomposites and nanocomposites containing the GOx complex was determined using statistical analysis of both images, indicating that the binding process did not affect the size of nanocomposites. Due to the immobilization of GOx on nanocomposites, this is obvious from the physical assessment of images without exhibiting extra aggregation.

3.7 VSM Analysis Results

One of the advantages of using magnetic structures as drug carriers is their ability to deliver the drug through an external magnetic field. Consequently, a comprehensive evaluation of the magnetic properties of these carriers becomes essential. Magnetic measurements of the nanoparticles were explored in an applied magnetic field at room temperature, with the field sweeping from –10,000 to +10,000 Oe using a VSM. As depicted in Fig. 12, the magnetization of Fe_2O_3/SiO_2 MNCs saturated up to 32.88 emu/g at an applied field of 10000 Oe.

* Figure 12 can be found in the Appendix section.

This behaviour indicates superparamagnetic characteristics at room temperature, [86], [119]. It means that the produced Fe_2O_3/SiO_2 MNCs are suitable for applications in biomedical diagnostics and therapy. These applications encompass a range of uses including contrast agents for magnetic resonance imaging (MRI), hyperthermia treatment, bio magnetic separation, as well as magnetic nanoparticles targeting and delivery.

3.8 Effects of Operational Conditions on the Yields of Photocatalytic Degradation for GOx Enzymatic Nano-Catalysts on Coated with Fe_2O_3/SiO_2 MNCs

3.8.1 Effect of Photocatalytic Degradation Time

Increasing photocatalytic degradation times (30, 60, 90, 120 and 150 min) were operated with photocatalytic degradation process for GOx enzymatic nano-catalysts on coated with Fe_2O_3/SiO_2 MNCs, at 300 W UV-vis light, and at 25ºC, respectively (Table 9).

* Table 9 can be found in the Appendix section.

99.11% maximum photocatalytic degradation removal yield was observed for 1.0 mg/l GOx enzymatic nano-catalyst concentration coated with 20 mg/l Fe_2O_3/SiO_2 MNCs, after 120 min, at 300 W UV-vis, and at 25ºC, respectively (Table 10).

3.8.2 Effect of Photodegradation Temperatures

The effects of Increasing temperatures (25, 50, 75, and 100ºC) on GOx photo-removal was examined coated with Fe_2O_3/SiO_2 MNCs after 120 min, and at 300 W UV-vis light, respectively (Table 11). 54.68%, 74.32%, and 50.14% GOX photocatalytic degradation removals yields at 0.1, 0.5, and 2.0 mg/l GOx doses was detected with 20 mg/l Fe_2O_3/SiO_2 MNCs concentration at 25ºC, at 75ºC, and at 100ºC, after 120 min, and at 300 W UV-vis light, respectively, (Table 10).

* Table 10 can be found in the Appendix section.

The maximum 99.45% GOx photocatalytic removal was obtained with 20 mg/l Fe_2O_3/SiO_2 MNCs concentration, at 50ºC, after 120 min, and at 300 W UV-vis light, respectively (Table 10).

3.8.3 Effect of pH Values

The effects of Increasing pH values (5.0, 7.0, 9.0 and 11.0) on photocatalytic removal of GOx was examined with 20 mg/l Fe_2O_3/SiO_2 MNCs after 120 min, at 300 W UV-vis light and at 50ºC, respectively (Table 12). 75.83%, 96.30%, and 94.05% GOx photocatalytic degradation efficiencies was measured at pH=5.0, pH=9.0 and pH=11.0, respectively, after 120 min, at 300 W UV-vis light, and at 50ºC, respectively (Table 11).

* Table 11 can be found in the Appendix section.

For 1.0 mg/l GOx concentration maximum 99.36% GOx photocatalytic degradation removal was obtained with 20 mg/l Fe_2O_3/SiO_2 MNCs at pH=7.0, after 120 min, at 300 W UV-vis light, and at 50ºC, respectively (Table 11).

The Photodegradation of GOx are affected by the pH of the solution. The variation of solution pH changes the surface charge of Fe_2O_3/SiO_2 MNCs particles and shifts the potentials of catalytic reactions. As a result, the adsorption of GOx on the surface is altered thereby causing a change in the reaction rate. Under acidic or alkaline condition, the surface of Fe_2O_3/SiO_2 MNCs can be protonated or deprotonated respectively. In acidic conditions the surface of the Fe_2O_3/SiO_2 MNCs will remain positively charged while in alkaline medium it will becomes negatively charged. At lower pH Fe_2O_3/SiO_2 MNCs exhibit higher oxidizing activity where as in higher pH level reaction rate will be decreased. Fe_2O_3/SiO_2 MNCs behaves as a strong acid due to the surface positive charge. In other words, the anionic dye acts as a strong Lewis base and can easily adsorb on the positively charged catalyst surface. This favours the adsorption of the GOx under acidic conditions, while in the alkaline conditions this complexation process is not favoured presumably because of competitive adsorption by hydroxyl groups and the GOx molecule in addition to the Columbic repulsion due to the negatively charged catalyst with the GOx molecule [19]. The extent of Gox adsorption depends on the initial GOx concentration, nature of the GOX surface area of photocatalyst and pH of the solution. The pH determines the surface charge of the photocatalyst. Adsorption of the GOx is minimum when the pH of the solution is at the isoelectric point (point of zero charge). The surface of the photocatalyst is positively charged below isoelectric point and carries a negative charge above it.

3.8.4 Effect of Fe_2O_3/SiO_2 MNCs Concentrations

The reactor system was operated at different Fe_2O_3/SiO_2 MNCs concentrations (5, 10, 15, 20 and 25 mg/l) to determine the removal yields of GOx enzymatic nano-catalyst was detected at 120 min, at

300 W UV-vis light, at pH=7.0 and at 50ºC, respectively (Table 12).

* Table 12 can be found in the Appendix section.

51.07%, 76.05%, 89.17%, 97.94% GOx photocatalytic degradation yields were found with 5 mg/l, at 10 mg/l, at 15 mg/l, and at 25 mg/l Fe_2O_3/SiO_2 MNCs, after 120 min, at 300 W UV-vis light, at pH=7.0 and at 50ºC, respectively (Table 12). Maximum 99.69% GOx photocatalytic degradation efficiency was obtained with 20 mg/l Fe_2O_3/SiO_2 MNCs, after 120 min, at 300 W UV-vis light, at pH=7.0 and at 50ºC, respectively (Table 12).

Rate of photocatalytic degradation effected also by the amount of catalyst. As increasing amount of catalyst in the photocatalytic process rate of photodegradation also enhanced. This can be explained on the basis that as increase in amount of catalyst commonly enhance the number of active sites on the surface of the photocatalyst thus causing an increase in the formation of number of •OH radicals which can take part in actual discoloration of dye solution. Beyond a certain limit of catalyst amount, the solution becomes turbid and thus blocks UV radiation for the reaction to proceed and therefore percentage degradation starts decreasing.

3.8.5 Effect of GOx Enzymatic Nano-Catalysts Concentrations

The effects of increasing GOx enzymatic nano-catalysts concentrations (0.1, 0.5, 1.0 and 2.0 mg/l) on GOx removal yields at 20 mg/l Fe_2O_3/SiO_2 MNCs concentration, after 120 min, at 300 W UV-vis light, at pH=7.0 and at 50ºC, respectively (Table 13).

* Table 13 can be found in the Appendix section.

49.08%, 73.45%, 97.38% GOx photocatalytic degradation yields were measured at 0.1 mg/l, at 0.5 mg/l, and 2.0 mg/l GOx enzymatic nano-catalyst concentrations, respectively, with 20 mg/l Fe_2O_3/SiO_2 MNCs, after 120 min, at 300 W UV-vis light, at pH=7.0 and at 50ºC, respectively (Table 13).

Maximum 99.04% photocatalytic degradation efficiency was obtained for GOx with at 1.0 mg/l GOx enzymatic nano-catalyst concentration, at 20 mg/l Fe_2O_3/SiO_2 MNCs, after 120 min, at 300 W UV-vis light, at pH=7.0 and at 50ºC, respectively (Table 13).

The initial concentration of GOx in a given photocatalytic reaction is an important factor which needs to be taken into account. Generally speaking, the percentage degradation decreases with increasing amount of GOx concentration, while keeping a fixed amount of catalyst]. This can be rationalized on the basis that as GOX concentration increases, more organic substances are adsorbed on the surface of Photocatalyst, whereas a smaller number of photons are available to reach the catalyst surface and therefore less •OH are formed, thus resulting in less degradation percentage. The photodegradation of GOx are increase with decreasing the concentration of GOx with the photocatalyst.

3.9 Determination of Kinetic Parameters of Immobilized GOx Enzymatic Nano-Catalysts Coated with Fe_2O_3 NCs Coated with SiO_2 NCs

For the determination of kinetic parameters, steady-state kinetics were performed for both the formulations (soluble and immobilized GOx) by varying the concentration of glucose at standard assay conditions. The Michaelis−Menten parameters (K_m and V_{max}) were calculated by converting the steady-state plot to a double reciprocal plot (Lineweaver Burk plot) as shown in Fig. 13.

* Figure 13 can be found in the Appendix section.

It has been observed from Table 14 that the calculated value of K_m was slightly increased (45.28 vs 58.29 mM) whereas V_{max} (1745.22 vs 969.93 μmol/min) decreases after immobilization. In comparison with soluble enzymes, immobilized GOx has a lower affinity toward glucose; it might be due to the diffusional limitation of the substrate to the active sites of immobilized GOx because of the nanocomposites.

* Table 14 can be found in the Appendix section.

The maximum rate of immobilized GOx is also lower than that of soluble GOx. The decreased V_{max} of GOx might be due to some conformational changes in the immobilized GOx due to conjugation with coated Fe_2O_3/SiO_2 MNCs, which affect either formation of an enzyme−substrate complex or the release of a product from the enzyme.

4 Conclusions

Microbial fuel cells and anaerobic digestion are promising bioenergy methods but inefficient and scalable. With its exceptional surface area-to-volume ratio, nano-catalysts are revolutionizing this field. Researchers have improved energy conversion efficiency by immobilizing or embedding nanoparticles on electrodes or catalytic supports to promote electron transport. Nanomaterials like Fe_2O_3 and SiO_2 and other metal nanoparticles speed up

organic matter breakdown and make bioenergy systems more profitable. Researchers are working harder to find new bioenergy-generating methods to address environmental concerns and the demand for sustainable energy.

The study discusses how nano-catalysts and enzymatic catalysts are revolutionizing bioenergy production in green energy. Additionally, enzymatic catalysts are the best bioenergy catalysts.

Highly specialized, biocompatible, and renewable enzymes provide unrivalled biofuel production potential. Protein engineering and immobilization have improved enzymes for bioenergy systems. Enzymatic catalysts enable biofuel generation from more feedstocks without harsh chemical procedures by controlling biological reactions quickly and precisely.

In this study, in order to perform bioenergy from GOx which is an oxidoreductase that catalyses the oxidation of β-D-glucose to D-glucono-δ-lactone a nano-catalyst namely Fe_2O_3/SiO_2 was used. In the lab-scale experimental study the GOx enzymatic nano-catalysts was coated with Fe_2O_3/SiO_2 MNCs to photodegrade GOx and the effects of some different experimental conditions on photocatalytic degradation efficiency was researched. The physicochemical properties of the Fe_2O_3/SiO_2 MNCs were investigated by XRD, FTIR, FE-SEM, EDX, UV-vis spectra, HRTEM and VSM analyses. The effects of some operational conditions such as photocatalytic degradation time, temperature, pH values, GOx enzymatic catalysis and Fe_2O_3/SiO_2 MNCs concentrations on the photocatalytic degradation efficiencies of an oxidoreductase that catalyses the oxidation of GOx (β-D-glucose to D-glucono-δ-lactone) were investigated.

99.69% maximum photocatalytic degradation efficiency was obtained for GOx enzymatic nano-catalysts with 20 mg/l Fe_2O_3/SiO_2 MNCs, after 120 min, at 300 W UV-vis light, at pH=7.0 and at 50ºC, respectively.

Combining nano-catalysts and enzymatic catalysts is promising. Nano-catalysts improve enzymatic processes by creating a favourable microenvironment, enhancing surface binding sites, and enabling substrate transport. This combination may maximize bioenergy systems' biofuel output and wastewater treatment capabilities.

Finally, to this study, integrating nano-catalysts and enzymatic catalysts is a green energy breakthrough. These advances will improve bioenergy generation by overcoming current techniques, opening new sustainable energy production prospects, and expediting our transition to a greener, more sustainable future.

Acknowledgement:
Experimental analyzes in this study were performed at the Laboratories of the Canada Research Center, Ottawa, Canada. The authors would like to thank this body for providing financial support.

References:

[1] W. W. Reid, M. K. Ali, C. B. Field, The Future of Bioenergy, *Global Change Biology*, Vol.26, 2020, pp. 274–286.

[2] I. Arya, A. Poona, P. K. Dikshit, S. Pandit, J. Kumar, H. N. Singh, N. K. Jha, H. A. Rudayni, A. A. Chaudhary, S. Kumar, Current Trends and Future Prospects of Nanotechnology in Biofuel Production, *Catalysts*, Vol.11, 2021, 1308.

[3] B. Cui, H. Peng, H. Xia, X. Guo, H. Guo, Magnetically Recoverable Core−Shell Nanocomposites γ-Fe_2O_3@SiO_2@TiO_2−Ag with Enhanced Photocatalytic Activity and Antibacterial Activity, *Separation and Purification Technology*, Vol.103, 2013, pp. 251−257.

[4] N. P. Sheehan, A. Ng, K. Murray, E. Martinez, K. Quell, C. Ouellette, T. Flagg, J. Boyle, Bioenergy from Biofuel Residues and Waste, *Water Environment Research*, Vol.92, 2020, pp. 1433–1439.

[5] Zulqarnain, M. Ayoub, M. H. M. Yusoff, M. H. Nazir, I. Zahid, M. Ameen, F. Sher, D. Floresyona, E. B. Nursanto, A Comprehensive Review on Oil Extraction and Biodiesel Production Technologies, *Sustainability*, Vol.13, 2021, 788.

[6] J. Pavicic, K. N. Mavar, V. Brkic, K. Simon, Biogas and Biomethane Production and Usage: Technology Development, Advantages and Challenges in Europe, *Energies*, Vol.15, 2022, 2940.

[7] Y. Kumar, P. Yogeshwar, S. Bajpai, P. Jaiswal, S. Yadav, D. P. Pathak, M. Sonker, S. K. Tiwary, Nanomaterials: Stimulants for Biofuels and Renewables, Yield and Energy Optimization, *RSC Materials Advances*, Vol.2, 2021, pp. 5318–5343.

[8] Z. Nasir, A. Ali, M. Shakir, R. Wahab, S. Shamsuzzaman, L. Lutfullah, Silica-Supported NiO Nanocomposites Prepared via a Sol Gel Technique and Their Excellent Catalytic Performance for One-Pot Multicomponent Synthesis of Benzodiazepine Derivatives under

Microwave Irradiation, *RSC New Journal of Chemistry*, Vol.41, 2017, pp. 5893−5903.

[9] L. Wang, C. Hu, L. Shao, The Antimicrobial Activity of Nanoparticles: Present Situation and Prospects for the Future, *International Journal of Nanomedicine*, Vol.12, 2017, pp. 1227−1249.

[10] M. Kooti, S. Gharineh, M. Mehrkhah, A. Shaker, H. Motamedi, Preparation and Antibacterial Activity of $CoFe_2O_4/SiO_2$/Ag Composite Impregnated with Streptomycin, *Chemical Engineering Journal*, Vol.259, 2015, pp. 34−42.

[11] M. Kooti, P. Kharazi, H. Motamedi, Preparation and Antibacterial Activity of Three-Component $NiFe_2O_4$@PANI@Ag Nano Composite, *Journal of Materials Science and Technology*, Vol.30, 2014a, pp. 656−660.

[12] M. Kooti, P. Kharazi, H. Motamedi, Preparation, Characterization, and Antibacterial Activity of $CoFe_2O_4$/Polyaniline/Ag Nano Composite, *Journal of the Taiwan Institute of Chemical Engineers*, Vol.45, 2014b, pp. 2698−2704.

[13] A. Kasinath, S. Fudala-Ksiazek, M. Szopinska, H. Bylinski, W. Artichowicz, A. Remiszewska-Skwarek, A. Luczkiewicz, Biomass in Biogas Production: Pretreatment and Co-Digestion, *Renewable and Sustainable Energy Reviews*, Vol.150, 2021, 111509.

[14] V. Shah, M. Patel, D. Patel, N. Patel, P. Prajapati, *Production of Biogas and the Associated Factors: A Guide for Successful Implementation of a Biogas Digester*, 4th Symposium on Industrial Science and Technology (SISTEC2022), Pahang, Malaysia, 2024, 040002.

[15] O. A. Aworanti, A. O. Ajani, O. O. Agbede, S. E. Agarry, O. Ogunkunle, O. T. Laseinde, M. A. Kalam, I. M. R. Fattah, Enhancing and Upgrading Biogas and Biomethane Production in Anaerobic Digestion: A Comprehensive Review, *Frontiers in Energy Research*, Vol.11, 2023, 1170133.

[16] D. Deublein, A. Steinhauser, *Biogas from Waste and Renewable Resources: An Introduction, Second,* Revised and Expanded edition, Weinheim: Wiley-VCH, 2011.

[17] E. Ryckebosch, M. Drouillon, H. Vervaeren, Techniques for Transformation of Biogas to Biomethane, *Biomass Bioenergy*, Vol.35, No.5, 2011, pp. 1633–1645.

[18] I. U. Khan, M. H. D. Othman, H. Hashim, T. Matsuura, A. F. Ismail, M. Rezaei-DashtArzhandi, W. Azelee, Biogas as a Renewable Energy Fuel – A Review of Biogas Upgrading, Utilisation and Storage, *Energy Conversion and Management*, Vol.150, 2017, pp. 277–294.

[19] Y. Cai, Z. Zheng, F. Schäfer, W. Stinner, X. Yuan, H. Wang, Z. Cui, X. Wang, A Review about Pretreatment of Lignocellulosic Biomass in Anaerobic Digestion: Achievement and Challenge in Germany and China, *Journal of Cleaner Production*, Vol.299, 2021, 126885.

[20] Q. Sun, H. Li, J. Yan, L. Liu, Z. Yu, X. Yu, Selection of Appropriate Biogas Upgrading Technology-A Review of Biogas Cleaning, Upgrading and Utilisation, *Renewable and Sustainable Energy Reviews*, Vol.51, 2015, pp. 521–532.

[21] I. Angelidaki, L. Treu, P. Tsapekos, G. Luo, S. Campanaro, H. Wenzel, P. G. Kougias, Biogas Upgrading and Utilization: Current Status and Perspectives, *Biotechnology Advances*, Vol.36, No.2, 2018, pp. 452–466.

[22] A. M. Buswell, H. F. Mueller, Mechanism of Methane Fermentation, *Industrial & Engineering Chemistry*, Vol.44, No.3, 1952, pp. 550–552.

[23] I. Rocamora, S. T. Wagland, R. Villa, E. W. Simpson, O. Fernandez, Y. Bajon-Fernandez, Dry Anaerobic Digestion of Organic Waste: A Review of Operational Parameters and Their Impact on Process Performance, *Bioresource Technology*, Vol.299, 2020, 122681.

[24] S. S. Bhajani, Review: Factors Affecting Biogas Production, *International Journal for Research in Applied Science and Engineering Technology*, Vol.10, No.2, 2022, pp. 79–88.

[25] M. Saraswat, M. Garg, M. Bhardwaj, M. Mehrotra, R. Singhal, Impact of Variables Affecting Biogas Production from Biomass, *IOP Conference Series: Materials Science and Engineering*, Vol.691, No.1, 2019, 012043.

[26] Yadvika, Santosh, T. R. Sreekrishnan, S. Kohli, V. Rana, Enhancement of Biogas Production from Solid Substrates Using Different Techniques—A Review, *Bioresource Technology*, Vol.95, No.1, 2004, pp. 1–10.

[27] C. Morales-Polo, M. D. M. Cledera-Castro, B. Y. Moratilla Soria, Reviewing the Anaerobic Digestion of Food Waste: from Waste Generation and Anaerobic Process to Its Perspectives, *Applied Sciences*, Vol.8, No.10, 2018, 1804.

[28] A. Hilkiah Igoni, M. J. Ayotamuno, C. L. Eze, S. O. T. Ogaji, S. D. Probert, Designs of Anaerobic Digesters for Producing Biogas from Municipal Solid-Waste, *Applied Energy*, Vol.85, No.6, 2008, pp. 430–438.

[29] G. Alemayehu, Co-Digestion of Municipal Organic Wastes with Night Soil and Cow Dung for Biogas Production: A Review, *African Journal of Biotechnology*, Vol.15, No.2, 2016, pp. 32–44.

[30] O. P. Karthikeyan, C. Visvanathan, Bio-Energy Recovery from High-Solid Organic Substrates by Dry Anaerobic Bio-Conversion Processes: A Review, *Reviews in Environmental Science and Bio/Technology*, Vol.12, No.3, 2013, pp. 257–284.

[31] B. Deepanraj, V. Sivasubramanian, S. Jayaraj, Effect of Substrate Pretreatment on Biogas Production through Anaerobic Digestion of Food Waste, *International Journal of Hydrogen Energy*, Vol.42, No.42, 2017, pp. 26522–26528.

[32] E. P. Sanchez, P. Weiland, L. Travieso, Effect of the Hydraulic Retention Time on the Anaerobic Biofilm Reactor Efficiency Applied to Screened Cattle Waste Treatment, *Biotechnology Letters*, Vol.14, No.7, 1992, pp. 635–638.

[33] M. Desai, D. Madamwar, Anaerobic Digestion of a Mixture of Cheese Whey, Poultry Waste and Cattle Dung: A Study of the Use of Adsorbents to Improve Digester Performance, *Environmental Pollution*, Vol.86, No.3, 1994, pp. 337–340.

[34] K. Karim, R. Hoffmann, K. Thomas Klasson, M. H. Al-Dahhan Anaerobic Digestion of Animal Waste: Effect of Mode of Mixing, *Water Research*, Vol.39, No.15, 2005, pp. 3597–3606.

[35] H. Bouallagui, H. Lahdheb, E. Ben Romdan, B. Rachdi, M. Hamdi, Improvement of Fruit and Vegetable Waste Anaerobic Digestion Performance and Stability with Co-Substrates Addition, *Journal of Environmental Management*, Vol.90, No.5, 2009, pp. 1844–1849.

[36] H. Li, C. Li, W. Liu, S. Zou, Optimized Alkaline Pretreatment of Sludge Before Anaerobic Digestion, *Bioresource Technology*, Vol.123, 2012, pp. 189–194.

[37] Zeshan, O. P. Karthikeyan, C. Visvanathan, Effect of C/N Ratio and Ammonia-N Accumulation in A Pilot-Scale Thermophilic Dry Anaerobic Digester, *Bioresource Technology*, Vol.113, 2012, pp. 294–302.

[38] M. Schnedlitz, M. Lasserus, R. Meyer, D. Knez, F. Hofer, W. E. Ernst, A. W. Hauser, Stability of Core–Shell Nanoparticles for Catalysis at Elevated Temperatures: Structural Inversion in the Ni–Au System Observed at Atomic Resolution, *Chemistry of Materials*, Vol.30, No.3, 2018, pp. 1113–1120.

[39] B. K. Shrestha, R. Ahmad, H. M. Mousa, I.-G. Kim, J. I. Kim, M. P. Neupane, C. H. Park, C. S. Kim, High-Performance Glucose Biosensor based on Chitosan-Glucose Oxidase Immobilized Poly Pyrrole/Nafion/Functionalized Multi-Walled Carbon Nanotubes Bio Nanohybrid Film, *Journal of Colloid and Interface Science*, Vol.482, 2016, pp. 39−47.

[40] B. E. Douglas, S. M. Ho, eds., Chapter 10: *Crystal Structures of Silica and Metal Silicates*, in Book: Structure and Chemistry of Crystalline Solids, New York, NY: Springer, doi:10.1007/0-387-36687-3_10, ISBN 978-0-387-36687-6, retrieved 2023-10-08, pp.233-278, 2006.

[41] M. Broda, D. J. Yelle, K. Serwanska, Bioethanol Production from Lignocellulosic Biomass-Challenges and Solutions, *Molecules*, Vol.27, 2022, 8717.

[42] S. B. Bankar, M. V. Bule, R. S. Singhal, L. Ananthanarayan, Glucose Oxidase an Overview, *Biotechnology Advances*, Vol.27, 2009, pp. 489−501.

[43] U. Ghoshdastider, R. Xu, B. Trzaskowski, K. Mlynarczyk, P. Miszta, S. Viswanathan, V. Renugopalakrishnan, S. Filipek, Molecular Effects of Encapsulation of Glucose Oxidase Dimer by Graphene, *RSC Advances*, Vol.5, No.18, 2015, pp. 13570–13578.

[44] C. M. Wong, K. H. Wong, X. D. Chen, Glucose Oxidase: Natural Occurrence, Function, Properties and Industrial Applications, *Applied Microbiology and Biotechnology*, Vol.78, No.6, 2008, pp. 927–938.

[45] Y. C. Yee, R. Hashim, A. R. Mohd Yahya, Y. Bustami, Colorimetric Analysis of Glucose Oxidase-Magnetic Cellulose Nano Crystals (CNCs) for Glucose Detection, *Sensors*, Vol.19, 2019, 2511.

[46] E. Afshari, S. Mazinani, S. O. Ranaei-Siadat, H. Ghomi, Surface Modification of Polyvinyl Alcohol/Malonic Acid Nanofibers by Gaseous Dielectric Barrier Discharge Plasma for Glucose Oxidase Immobilization, *Applied Surface Science*, Vol.385, 2016, pp. 349−355.

[47] A. Agi, R. Junin, M. Z. Jaafar, R. Mohsin, A. Arsad, A. Gbadamosi, J. Gbonhinbor, Synthesis and Application of Rice Husk Silica Nanoparticles for Chemical Enhanced Oil Recovery, *Journal of Materials Research and Technology*, Vol.9, No.6, 2020, pp. 13054-13066.

[48] W. Y. Cheah, R. Sankaran, P. L. Show, T. N. B. T. Ibrahim, K. W. Chew, A. Culaba, J. S. Chang, Pretreatment Methods for Lignocellulosic

Biofuels Production: Current Advances, Challenges and Future Prospects, *Biofuel Research Journal*, Vol.7, No.1, 2020, pp. 1115–1127.

[49] D. Ramutshatsha-Makhwedzha, J. C. Ngila, P. G. Ndungu, P. N. Nomngongo, Ultrasound Assisted Adsorptive Removal of Cr, Cu, Al, Ba, Zn, Ni, Mn, Co and Ti from Seawater Using Fe_2O_3-SiO_2-PAN Nanocomposite: Equilibrium Kinetics, *Journal of Marine Science and Engineering*, Vol.7, No.5, 2019, 133.

[50] J. Raba, H. A. Mottola, Glucose Oxidase as an Analytical Reagent, *Critical Reviews in Analytical Chemistry*, Vol.25, No.1, 1995, pp. 1–42.

[51] Z. Islam Rony, M. Mofijur, M. M. Hasan, M. G. Rasul, M. I. Jahirul, S. F. Ahmed, M. A. Kalam, I. A., Badruddin, T. M. Yunus Khan, P.-L. Show, Alternative Fuels to Reduce Greenhouse Gas Emissions from Marine Transport and Promote UN Sustainable Development Goals, *Fuel*, Vol.338, 2023, 127220

[52] A. Miri, H. Najafzadeh, M. Darroudi, M. J. Javad Miri, M. A. J. Kouhbanani, M. Sarani, Iron Oxide Nanoparticles: Biosynthesis, Magnetic Behaviour, Cytotoxic Effect, *ChemistryOpen*, Vol.10, No.3, 2021, pp. 327-333.

[53] M. François, K.-S. Lin, N. Rachmadona, K. S. Khoo, Advancement of Nanotechnologies in Biogas Production and Contaminant Removal: A Review, *Fuel*, Vol.340, 2023, 127470.

[54] A. V. Samrot, C. S. Sahithya, J. Selvarani, S. K. Purayil, P. Ponnaiah, A Review on Synthesis, Characterization and Potential Biological Applications of Superparamagnetic Iron Oxide Nanoparticles, *Current Research in Green and Sustainable Chemistry*, Vol.4, 2021, 100042.

[55] R. Ganesan, S. Manigandan, M. S. Samuel, R. Shanmuganathan, K. Brindhadevi, N. T. L. Chi, P. A. Duc, A. Pugazhendhi, A Review on Prospective Production of Biofuel from Microalgae, *Biotechnology Reports*, Vol.27, 2020, e00509.

[56] B. Kumar, K. Smita, S. Galeas, V. H. Guerrero, A. Debut, L. Cumbal, One-Pot Biosynthesis of Maghemite (γ-Fe_2O_3) Nanoparticles in Aqueous Extract of Ficus Carica Fruit and Their Application for Antioxidant and 4-Nitrophenolreduction, *Waste and Biomass Valorization*, Vol.12, 2021, pp. 3575–3587.

[57] Y. Kanna Dasan, M. K. Lam, Y. H. Chai, J. W. Lim, Y. C. Ho, I. S. Tan, S. Y. Lau, P. L. Show, K. T. Lee, Unlocking the Potential of Microalgae Bio-Factories for Carbon Dioxide Mitigation: A Comprehensive Exploration of Recent Advances, Key Challenges, and Energy-Economic Insights, *Bioresource Technology*, Vol.380, 2023, 129094.

[58] M. J. Borah, A. Das, V. Das, N. Bhuyan, D. Deka, Transesterification of Waste Cooking Oil for Biodiesel Production Catalysed by Zn Substituted Waste Egg Shell Derived CaO Nanocatalyst, *Fuel*, Vol.242, 2019, pp. 345-354.

[59] J. Amin Ahmed Abdullah, L. Salah Eddine, B. Abderrhmane, M. Alonso-González, A. Guerrero, A. Romero, Green Synthesis and Characterization of Iron Oxide Nanoparticles by Pheonix Dactylifera Leaf Extract and Evaluation of Their Antioxidant Activity, *Sustainable Chemistry and Pharmacy*, Vol.17, 2020, 100280.

[60] A. Kumar Rajak, S. Dalal, M. Harikrishna, U. Kumar Sahoo, M. S. L. Karuna, P. Kumar Sarangi, A Comprehensive Review of Biomass-Derived Heterogeneous Catalysts for Efficient Biodiesel Production, *Asian Journal of Water, Environmet and Pollution*, 2025, 025130095, pp. 1-54.

[61] S. S. Hosseini, M. A. Tabar, I. F. J. Vankelecom, J. Denayer, Progress in High Performance Membrane Materials and Processes for Biogas Production, Upgrading and Conversion, *Journal Separation and Purification Technology*, Vol.310, 2023, 123139, pp. 1-50.

[62] G. An, X. Zhang, C. Zhang, H. Gao, S. Liu, G. Qin, H. Qi, J. Kasemchainan, J. Zhang, G. Wang, Metal-Organic-Framework-Based Materials as Green Catalysts for Alcohol Oxidation, *Chinese Journal of Catalysis*, Vol.50, 2023, pp. 126-174.

[63] Z. Chen, Y. Xie, S. Qiu, M. Li, W. Yuan, S. Ge, Granular Indigenous Microalgal-Bacterial Consortium for Wastewater Treatment: Establishment Strategy, Functional Microorganism, Nutrient Removal, and Influencing Factor, *Bioresource Technology*, Vol.353, 2022, 127130.

[64] A. Allafchian, S. A. H. Jalali, H. Bahramian, H. Ahmadvand, Preparation, Characterization, and Antibacterial Activity of $NiFe_2O_4$/PAMA/Ag−TiO_2 Nanocomposite, *Journal of Magnetism and Magnetic Materials*, Vol.404, 2016, pp. 14−20.

[65] H. Adamu, U. Bello, A. U. Yuguda, U. I. Tafida, A. M. Jalam, A. Sabo, M. Qamar, Production Processes, Techno-Economic and Policy Challenges of Bioenergy Production from Fruit and Vegetable Wastes, *Renewable and Sustainable Energy Reviews*, Vol.186, 2023, 113686.

[66] I. M. Apetrei, M. L. Rodriguez-Mendez, C. Apetrei, J. A. de Saja, Enzyme Sensor Based on Carbon Nanotubes/Cobalt(II) Phthalo Cyanine and Tyrosinase used in Pharmaceutical Analysis, *Sensors & Actuators, B: Chemical*, Vol.177, 2013, pp. 138−144.

[67] I. K. Battisha, Structural and Optical Properties of Monolithic Silica-Gel Glasses Containing Nd+3 using Two Different Precursors TEOS and TMOS Prepared by Sol-Gel Technique, *Indian Journal of Pure and Applied Physics*, Vol.40, 2002, pp. 122−131.

[68] M. Kahoush, N. Behary, A. Cayla, B. Mutel, J. Guan, V. Nierstrasz, Surface Modification of Carbon Felt by Cold Remote Plasma for Glucose Oxidase Enzyme Immobilization, *Applied Surface Science,* Vol.476, 2019, pp. 1016−1024.

[69] S. Joarder, D. Bansal, H. Meena, N. Kaushik, J. Tomar, K. Kumari, I. Bahadur, E. H. Choi, N. Kumar Kaushik, P. Singh, Bioinspired Green Deep Eutectic Solvents: Preparation, Catalytic Activity, and Biocompatibilityi *Journal of Molecular Liquids*, Vol.376, 2023, 121355.

[70] M. N. Norizan, M. H. Moklis, S. Z. N. Demon, N. A. Halim, A. Samsuri, I. S. Mohamad, V. F. Knight, N. Abdullah, Carbon Nanotubes: Functionalisation and Their Application in Chemical Sensors, *RSC Advances*, Vol.10, 2020, pp. 43704–43732.

[71] W. Cai, M. Guo, X. Weng, W. Zhang, G. Owens, Z. Chen, Modified Green Synthesis of Fe_3O_4@SiO_2 Nanoparticles for pH Responsive Drug Release, *Materials Science & Engineering C-Materials for Biological Applications*, Vol.112, 2020, 110900.

[72] L. D. Fernández, E. Lara, E. A. Mitchell, Checklist, Diversity and Distribution of Testate Amoebae in Chile, *European Journal of Protistology*, Vol.51, No.5, 2015, pp. 409–424.

[73] T. T. Nguyen, H. T. Ma, P. Avti, M. J. Bashir, C. A. Ng, L. Y. Wong, N. Q. Tran, Adsorptive Removal of Iron Using SiO_2 Nanoparticles Extracted from Rice Husk Ash, *Journal of Analytical Methods in Chemistry*, 2019, pp. 1-9.

[74] A. Jędrzak, T. Rębis, M. Kuznowicz, A. Kołodziejczak Radzimska, J. Zdarta, A. Piasecki, T. Jesionowski, Advanced Ga_2O_3/Lignin and ZrO_2/Lignin Hybrid Microplatforms for Glucose Oxidase Immobilization: Evaluation of Biosensing Properties by Catalytic Glucose Oxidation, *Catalysts*, Vol.9, 2019b, 1044.

[75] R. Li, X. Fan, Y. F. Jiang, R. N. Wang, R. B. Guo, Y. Zhang, S. F. Fu, From Anaerobic Digestion to Single Cell Protein Synthesis: A Promising Route beyond Biogas Utilization, *Water Research*, Vol.243, 2023, 120417, pp. 1-15.

[76] A. A. Homaei, R. Sariri, F. Vianello, R. Stevanato, Enzyme Immobilization: An Update, *Journal of Biological Chemistry*, Vol.6, 2013, pp. 185−205.

[77] D. Keilin, E. F. Hartree, Specificity of Glucose Oxidase (Notatin), *The Biochemical Journal*, Vol.50, No.3, 1952, pp. 331–41.

[78] A. A. Laskar, M. F. Alam, H. Younus, In Vitro Activity and Stability of Pure Human Salivary Aldehyde Dehydrogenase, *International Journal of Biological Macromolecules*, Vol.96, 2017, pp. 798−806.

[79] H. Ono, T. Katsumata, Interfacial Reactions between Thin Rare Earth-Metal Oxide Films and Si Substrates, *Applied Physics Letters*, Vol.78, 2001, pp. 1832−1834.

[80] E. H. Ozkan, N. Sarı, Use of Immobilized Novel Dendritic Molecules as a Marker for the Detection of Glucose in Artificial Urine, *Journal of Molecular Structure*, Vol.120, 2020, 127134.

[81] H. Song, Metal Hybrid Nanoparticles for Catalytic Organic and Photochemical Transformations, *ACS Accounts of Chemical Research*, Vol.48, 2015, pp. 491–499.

[82] P. D. Maniar, A. Navrotsky, E. M. Rabinovich, J. Y. Ying, J. B. Benziger, Energetics and Structure of Sol-Gel Silicas, *Journal of Non-Crystalline Solids*, Vol.124, 1990, pp. 101−111.

[83] G. L. Miller, Use of Dinitrosalicylic Acid Reagent for Determination of Reducing Sugar, *Analytical Chemistry*, Vol.31, 1959, pp. 426−428.

[84] N. Narayan, A. Meiyazhagan, R. Vajtai, Metal Nanoparticles as Green Catalysts, *Materials*, Vol.12, No.21, 2019, 3602.

[85] K.-J. Kim, K. Y. Kim, G. B. Rhim, M. H. Youn, Y.-L. Lee, D. H. Chun, H.-S. Roh, Nano-Catalysts for Gas to Liquids: A Concise Review, *Chemical Engineering Journal*, Vol.468, 2023, 143632.

[86] N. Shahabadi, S. Zendehcheshm, M. Mahdavi, Synthesis of Se Nanoclusters via Ostwald Ripening Process: In Vitro Antibacterial and Antioxidant Activity, *Emergent Materials*, Vol.6, 2023, pp. 185–195.

[87] B. Behera, K. V. Supraja, B. Paramasivan, Integrated Microalgal Biorefinery for the Production and Application of Biostimulants in Circular Bioeconomy, *Bioresource Technology*, Vol.339, 2021, 125588.

[88] I. Z. Vass, Z. Deák, K. Paul, S. Kovács, I. Vass, Interaction of Nanoparticles with Biological

Systems, *Acta Biologica Szegediensis*, Vol.59, 2015, pp. 225−245.

[89] D. S. Barcellos, M. Procopiuck, H. A. Bollmann, Management of Pharmaceutical Micropollutants Discharged in Urban Waters: 30 years of Systematic Review Looking at Opportunities for Developing Countries, *Science of the Total Environment*, Vol.809, 2022, 151128.

[90] P. K. Smith, R. I. Krohn, G. T. Hermanson, A. K. Mallia, F. H. Gartner, M. D. Provenzano, E. K. Fujimoto, N. M. Goeke, B. J. Olson, D. C. Klenk, Measurement of Protein Using Bicinchoninic Acid, *Analytical Biochemistry*, Vol.150, 1985, pp. 76−85.

[91] S. S. Nekrashevich, V. A. Gritsenko, Electronic Structure of Silicon Dioxide (A Review), *Physics of the Solid State,* Vol.56, No.2, 2024, pp. 207–222.

[92] A. V. Rao, P. B. Wagh, D. Haranath, P. B. Risbud, S. D. Kumbhare, Influence of Temperature on the Physical Properties of TEOS Silica Xerogels, *Ceramics International*, Vol.25, 1999, pp. 505−509.

[93] Z. Nasir, A. Ali, F. Alam, Md. M. Shoeb, S. N. Jahan, Immobilization of GOx Enzyme on SiO_2-Coated Ni–Co Ferrite Nanocomposites as Magnetic Support and Their Antimicrobial and Photocatalytic Activities, *ACS Omega*, Vol.6, No.49, 2021, pp. 33554-33567.

[94] Z. Yue, J. Zhou, L. Li, H. Zhang, Z. Gui, Synthesis of Nanocrystalline NiCuZn Ferrite Powders by Sol-Gel Combustion Method, *Journal of Magnetism and Magnetic Materials*, Vol.208, 2000, pp. 55–60.

[95] K. V. Manukyan, A. Cross, S. Roslyakov, S. Rouvimov, A. S. Rogachev, E. E. Wolf, A. S. Mukasyan, Solution Combustion Synthesis of Nano-Crystalline Metallic Materials: Mechanistic Studies, *The Journal of Physical Chemistry C*, Vol.117, No.46, 2013, pp. 24417–24427.

[96] M. Kaliva, C. Gabriel, C. P. Raptopoulou, A. Terzis, G. Voyiatzis, M. Zervou, C. Mateescu, A. Salifoglou, A Unique Dinuclear Mixed V(V) Oxo-peroxo Complex in the Structural Speciation of the Ternary V(V)-Peroxo citrate System. Potential Mechanistic and Structural Insight into the Aqueous Synthetic Chemistry of Dinuclear V(V)-Citrate Species with H_2O_2, *Inorganic Chemistry*, Vol.50, 2011, pp. 11423–11436.

[97] A. L. Greer, Confusion by Design, *Nature*, Vol.366, 1993, pp. 303–304.

[98] S. R. Shinde, S. B. Ogale, J. S. Higgins, H. Zheng, A. J. Millis, V. N. Kulkarni, R. Ramesh, R. L. Greene, T. Venkatesan, Co-Occurrence of Superparamagnetism and Anomalous Hall Effect in Highly Reduced Cobalt-Doped Rutile $TiO_{2-\delta}$ films, *Physical Review Letters*, Vol.92, 2004, 166601.

[99] H. Bakhshi, N. Vahdati, A. Sedghi, Y. Mozharivskyj, Comparison of the Effect of Nickel and Cobalt Cations Addition on the Structural and Magnetic Properties of Manganese-Zinc Ferrite Nanoparticles, *Journal of Magnetism and Magnetic Materials*, Vol.474, 2019, pp. 56–62.

[100] R. Qin, F. Li, L. Liu, W. Jiang, Synthesis of Well-Dispersed $CoFe_2O_4$ Nanoparticles via PVA-Assisted Low-Temperature Solid State Process, *Journal of Alloys and Compounds*, Vol.482, 2009, pp. 508–511.

[101] A. V. Raut, R. S. Barkule, D. R. Shengule, K. M. Jadhav, Synthesis, Structural Investigation and Magnetic Properties of Zn^{2+} Substituted Cobalt Ferrite Nanoparticles Prepared by the Sol–Gel Auto-Combustion Technique, *Journal of Magnetism and Magnetic Materials*, Vol.358, 2014, pp. 87–92.

[102] W. C. Lipps, E. B. Braun-Howland, T. E. Baxter, T.E. *Standard Methods for the Examination of Water and Wastewater*, 24th. Edition, W. C. Lipps, E. B. Braun-Howland, T. E. Baxter, (editors), American Public Health Association (APHA), American Water Works Association (AWWA), Water Environment Federation (WEF), Elevate Your Standards. American Public Health Association 800 I Street, NW Washington DC: 20001-3770, USA, December 1, 2022; ISBN:9780875532998, 2022.

[103] J. H. Zar, *Biostatistical Analysis*, Prentice-Hall, Englewood Cliffs, 1984.

[104] *Statgraphics Centurion XV*, sofware, StatPoint Inc, Statgraphics Centurion XV, Herndon, VA, USA, 2005.

[105] C. Huang, X. Jiang, X. Shen, J. Hu, W. Tang, X. Wu, A. Ragauskas, H. Jameel, X. Meng, Q. Yong, Lignin-Enzyme Interaction: A Roadblock for Efficient Enzymatic Hydrolysis of Lignocellulosics, *Renewable and Sustainable Energy Reviews*, Vol.154, 2022, 111822.

[106] N. Dey, G. Kumar, A. S. Vickram, M., Mohan, R. R. Singhania, A. Kumar Patel, C.-D. Dong, K. Anbarasu, S. Thanigaivel, V. Kumar Ponnusamy, Nanotechnology-Assisted Production of Value-Added Biopotent Energy-Yielding Products from Lignocellulosic Biomass Refinery – A Review, *Bioresource Technology*, Vol.344, Part A, 2022, 126171.

[107] L. Cao, K. M. Iris, Y. X. Xiong, D. C. W. Tsang, S. Zhang, J. H. Clark, C. Hu, Y. H. Ng, J. Shang, Y. S. Ok, Biorenewable Hydrogen Production through Biomass Gasification: A Review and Future Prospects, *Environmental Research*, Vol.186, 2020, 109547.

[108] D. Chakraborty, S. Chatterjee, A. Althuri, S. G. Palani, V. Mohan, Sustainable Enzymatic Treatment of Organic Waste in a Framework of Circular Economy, *Bioresource Technology*, Vol.370, 2023, 128487.

[109] H. Lee, Y. J. Sohn, S. Jeon, H. Yang, J. Son, Y. J. Kim, S. J. Park, Sugarcane Wastes as Microbial Feedstocks: A Review of the Biorefinery Framework from Resource Recovery to Production of Value-Added Products, *Bioresource Technology*, Vol.376, 2023, 128879.

[110] W. Ding, G. Zhou, S. Wen, J. Yin, C. Liu, Y. Fu, L. Zhang, Two-Dimensional Activated Carbon Nanosheets for Rapid Removal of Tetracycline via Strong π-π Electron Donor Receptor Interactions, *Bioresource Technology*, Vol.360, 2022, 127544.

[111] F. Ale Enriquez, B. K. Ahring, Strategies to Overcome Mass Transfer Limitations of hydrogen during Anaerobic Gaseous Fermentations: A Comprehensive Review, *Bioresource Technology*, Vol.377, 2023, 128948.

[112] X. Deng, D. Luo, A. Okamoto, Defined and Unknown Roles of Conductive Nanoparticles for the Enhancement of Microbial Current Generation: A Review, *Bioresource Technology*, Vol.350, 2022, 126844.

[113] M. P. Ajith, M. Aswathi, E. Priyadarshini, P. Rajamani, Recent Innovations of Nanotechnology in Water Treatment: A Comprehensive Review, *Bioresource Technology*, Vol.342, 2021, 126000.

[114] S. Babu, S. S. Rathore, R. Singh, S. Kumar, V. K. Singh, S. K. Yadav, V. Yadav, R. Raj, D. Yadav, K. Shekhawat, Q. A. Wani, Exploring Agricultural Waste Biomass for Energy, Food and Feed Production and Pollution Mitigation: A Review, *Bioresource Technology*, Vol.360, 2022, 127566.

[115] M. Kumar Awasthi, P. Ganeshan, N. Gohil, V. Kumar, V. Singh, K. Rajendran, S. Harirchi, M. Kumar Solanki, R. Sindhu, P. Binod, Z. Zhang, M. J. Taherzadeh, Advanced Approaches for Resource Recovery from Wastewater and Activated Sludge: A Review, *Bioresource Technology*, Vol.384, 2023, 129250.

[116] N. Duan, B. Dong, B. Wu, X. Dai, High-Solid Anaerobic Digestion of Sewage Sludge under Mesophilic Conditions: Feasibility Study, *Bioresource Technology*, Vol.104, 2012, pp. 150–156.

[117] C. Veluchamy, B. H. Gilroyed, A. S. Kalamdhad, Process Performance and Biogas Production Optimizing of Mesophilic Plug Flow Anaerobic Digestion of Corn Silage, *Fuel*, Vol.253, 2019, pp. 1097–103.

[118] Y. Hu, J. Wu, H. Li, S. Poncin, K. Wang, J. Zuo, Study of An Enhanced Dry Anaerobic Digestion of Swine Manure: Performance and Microbial Community Property, *Bioresource Technology*, Vol.282, 2019, pp. 353–360.

[119] L. A. Fdez-Güelfo, C. Alvarez-Gallego, D. Sales Marquez, L. I. Romero García, Start-up of Thermophilic–Dry Anaerobic Digestion of OFMSW using Adapted Modified SEBAC Inoculum, *Bioresource Technology*, Vol.101, No.23, 2010, pp. 9031–9039.

[120] P. Ghosh, A. Singh, Physicochemical and Biological Treatments for Enzymatic/Microbial Conversion of Lignocellulosic Biomass, *Advances in Applied Microbiology*, Vol.39, 1993, pp. 295–333.

Contribution of Individual Authors to the Creation of a Scientific Article (Ghostwriting Policy)

Prof. Dr. Delia Teresa Sponza and Post-Dr. Rukiye Öztekin took an active role in every stage of the preparation of this article.

The authors equally contributed in the present research, at all stages from the formulation of the problem to the final findings and solution.

Sources of Funding for Research Presented in a Scientific Article or Scientific Article Itself

The experimental phases of this research study were conducted at the National Research Council (NRC) of Canada, Research Centers, Ontario, Canada. The authors would like to thank this body for providing financial support.

Conflict of Interest

The authors have no conflicts of interest to declare that are relevant to the content of this article.

APPENDIX

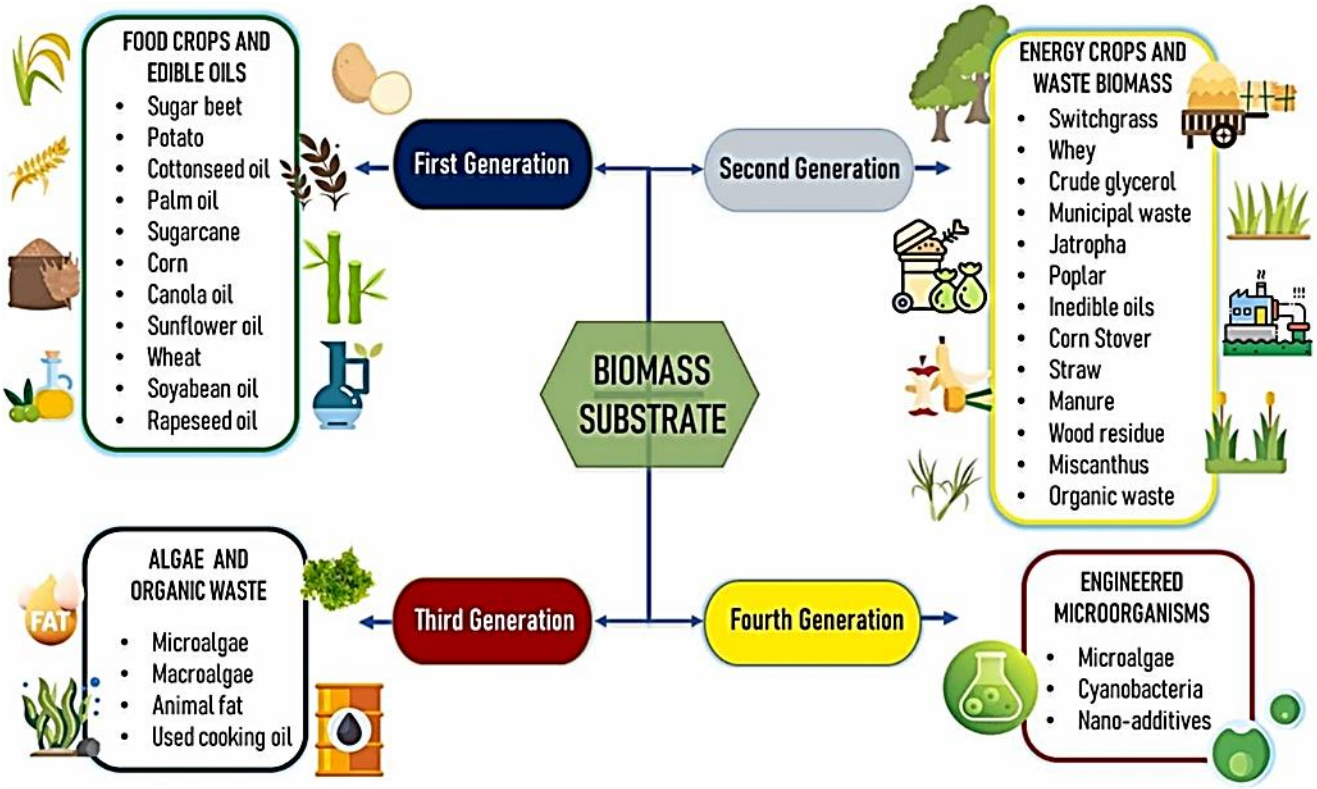

Figure 1. The conversion of biomass to substrate (First, Second, Third and Fourth Generations)

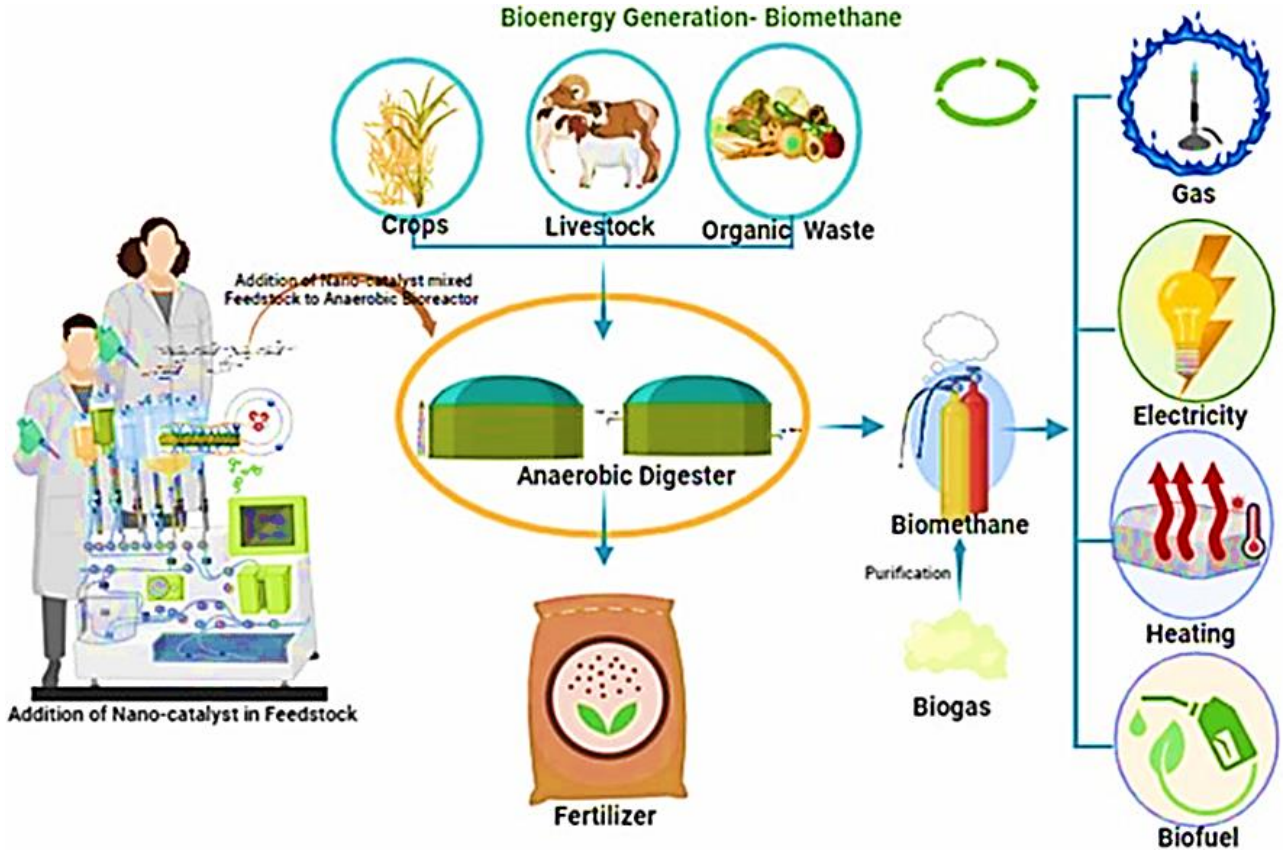

Figure 2. Bioenergy Generation from Biomethane

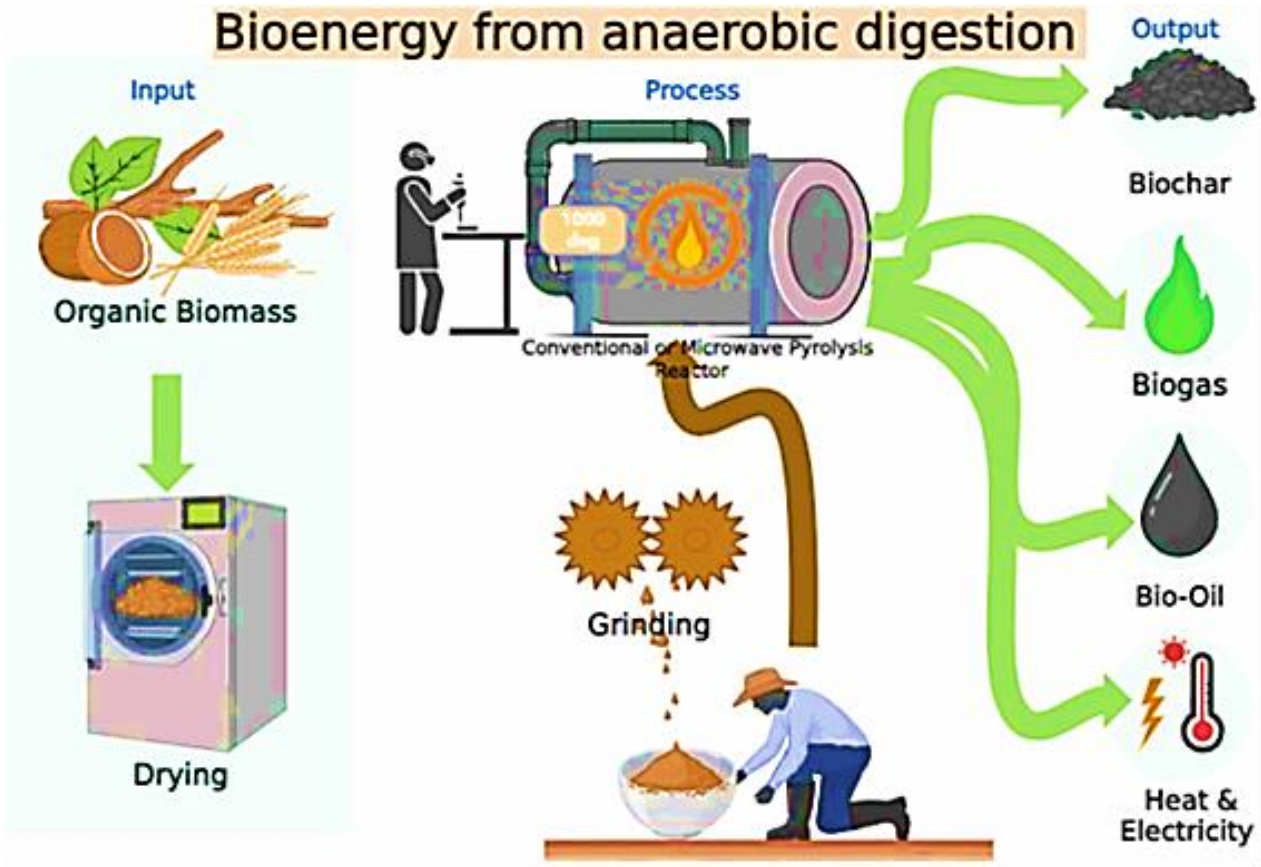

Figure 3. A Schematic Representation of Bioenergy from AD.

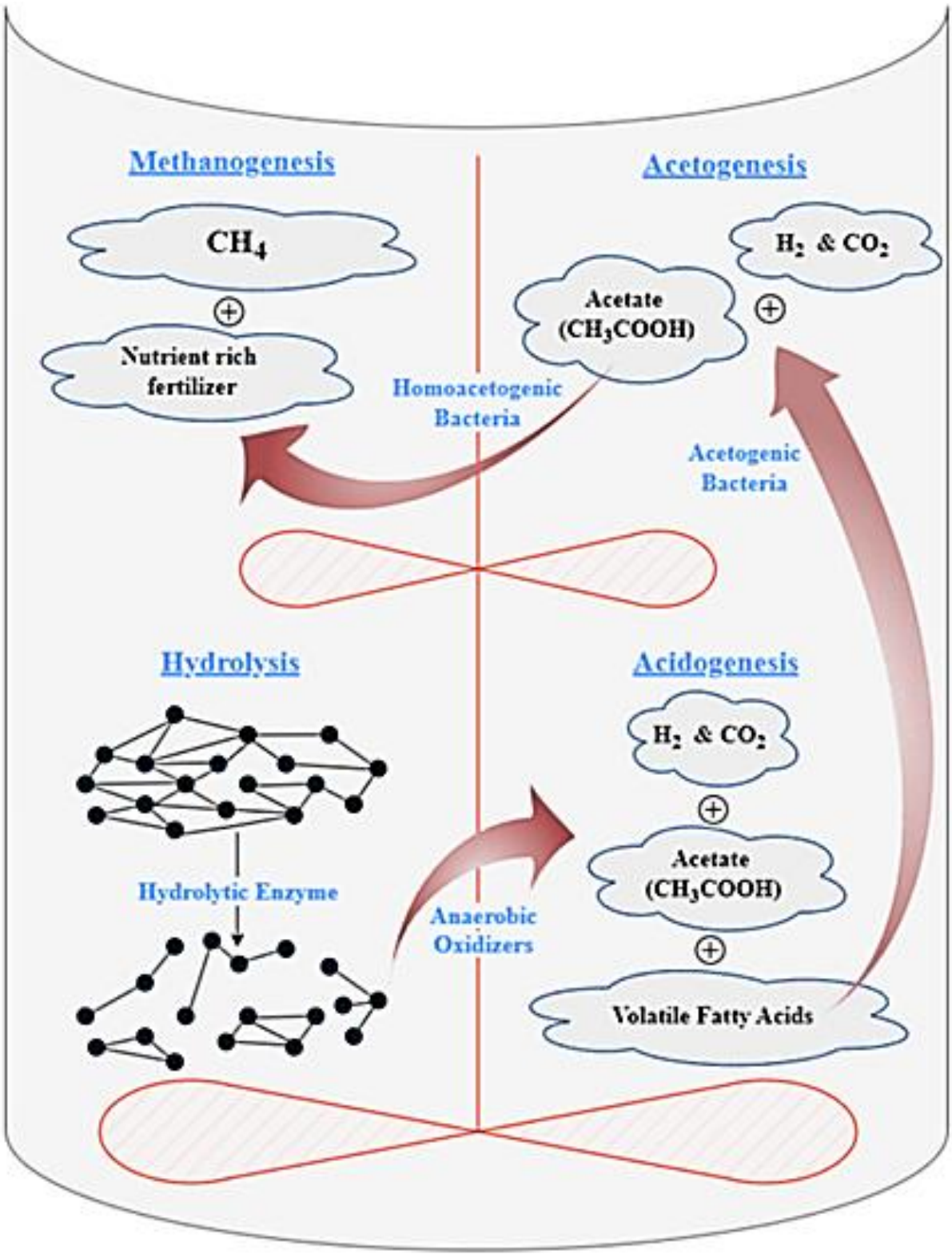

Figure 4. The schematic biodegradation steps of complex organic matter.

Table 1. The typical composition of raw biogas from waste [15], [20], [21].

Component	**Symbols**	**Concentration (vol.%)**
Methane	CH_4	45 – 75
Carbon dioxide	CO_2	25 – 50
Hydrogen sulfide	H_2S	< 2 (0 – 10,000 ppm)
Carbon monoxide	CO	Negligible
Ammonia	NH_3	< 1 (0 – 100 ppm)
Water vapor	$H_2O(g)$	1 – 10
Nitrogen	N_2	0 – 15
Oxygen	O_2	0 – 3
Hydrogen	H_2	Negligible
Siloxanes	$H(OSiH_2)nOH$ & $(OSiH_2)n$	0.02

Table 2. The optimum values of OLR & the yield of CH_4 for different substrates, [24].

Substrates	**OLR ($kgVS/m^3/day$)**	**Yield of CH_4 ($m^3/kgVS_{destroyed}$)**	**References**
Sewage sludge	8.5	0.190	[115]
Corn silage	3.5 – 8.5	0.327 – 0.410	[116]
Swine manure	4 - 8	0.050 – 0.450	[118]
Organic fraction of municipal solid waste	11.8	0.097	[119]

Table 3. The characteristics of various organic waste, [30], [117].

Organic waste	**Cellulose (%)**	**Hemi-cellulose (%)**	**Lignin (%)**
Corn stover	37.5	22.4	17.6
Corn fiber	14.3	16.8	8.4
Wheat straw	38.2	21.2	23.4
Leaves	15 - 20	80 - 85	NA
Bagasse	38.2	27.1	20.2
Sugarcane	25	17	12
Rice straw	32	24	13
Cattle manure	1.6 – 4.7	1.4 – 3.3	2.7 – 5.7
MSW	33	9	17
OF-MSW	60	20	20
Newspaper	62.1	16.1	21.1
Waste paper from pulps	60 - 70	10 - 20	5 – 10
Coffee pulp	35	46.3	18.8
Algae	20 - 40	20 - 50	NA
Banana waste	13.2	14.8	14
Nut shells	25 - 30	25 - 30	30 - 40

Table 4. Various organic waste with its C/N ratio, [30].

Organic waste	**C/N ratio (%)**	**Organic waste**	**C/N ratio (%)**
Corn stover	60 - 120	MSW	40
Corn fibre	35 - 45	OF-MSW	14 – 16
Wheat straw	90	Newspaper	175
Leaves	8 – 20	Waste paper from pulps	90
Bagasse	150	Coffee pulp	18.5
Sugarcane	50	Algae	19
Rice straw	70	Banana waste	21 – 34
Cattle manure	24	Nutshells	35

Table 5. Nano-catalysts revolutionizing bioenergy applications

Catalyst Type	Applications	Advantages	Challenges	References
Nanoparticles	Biofuel production catalytic conversion of biomass	High surface area, enhanced reactivity, tuneable properties	Agglomeration, stability under harsh conditions	[101]
Nanowires	Hydrogen production, photovoltaics, biofuel synthesis	High aspect ratio, efficient charge transport	Synthesis complexity, potential toxicity	[102]
Nanotubes	Fuel cell catalysts, hydrogen storages	High conductivity, large surface area	Dispersion in matrices, catalyst poisoning	[101]
Nanorods	Photocatalysis for water splitting, biofuel cells	Shape-dependent catalytic activity, improved light absorption	Synthesis control, stability in corrosive environments	[103]
Nanoclusters	Catalytic reduction reactions, biofuel upgrading	High catalytic activity, precise control	Stability, cost-effective synthesis	[104]
Nanocomposites	Energy storage materials, catalyst support	Enhanced catalytic performance, synergistic effects	Compatibility of components, scalability	[108]
Nanoporous	Gas storage, adsorption-based separation	High surface area, tuneable pore size	Synthesis complexity, durability	[110]
Core-Shell Nanoparticles	Biodiesel production, catalytic reactions	Enhanced stability, selectivity	Synthesis control, core-shell interface	[115]
Quantum Dots	Photovoltaics, Bioimaging	Size-tuneable electronic properties, efficient charge separation	Toxicity concerns, production cost	[116]

Table 6. Optimizing microenvironments for enhanced catalysis.

Catalyst Type	**Applications**	**Microenvironment Modification**	**Advantages**	**References**
Enzymatic Catalysts	Bioremediation, Biofuel production	pH adjustment, co-factor addition	Specificity, biocompatibility	[103]
Nanoparticles	Catalytic conversion, nanoscale reactions	Surface functionalization, size control	High reactivity, tuneable properties	[106]
Nanowires	Energy conversion, electrocatalysis	Surface modification, doping	Efficient charge transfer, tailored properties	[107]
Nanotubes	Drug delivery, nanoreactors	Surface functionalization, interior channel modification	Controlled release, high surface area	[104]
Nanorods	Photocatalysis, sensing	Aspect ratio adjustment, surface coating	Enhanced light absorption, stability	[106]

Table 7. The conventional techniques for wastewater treatment

Catalyst Type	**Applications**	**Microenvironment Modification**	**Advantages**	**References**
Climate Change Resilience	Integrated water management strategies, Adaptation of treatment infrastructure for changing weather patterns	Reduced vulnerability to extreme weather events, Sustainable water supply.	Requires long-term planning and investment. Uncertainty in future climate projections	[107]
Regulatory Compliance	Real-time monitoring and control systems, Regular audits and reporting.	Time adjustments to treatment processes, Demonstration of compliance to regulatory authorities.	High initial investment in monitoring systems. Stringent regulatory standards and penalties for non-compliance.	[108]
Resource Recovery	Phosphorus recovery from wastewater. Water reuse for non-potable applications.	Reduced dependence on external resources. Sustainable use of water and nutrients.	Technological and economic challenges in nutrient recover. Public perception and acceptance of water reuse.	[109]

Table 8. Comparison of Fe_2O_3/SiO_2 MNCs applications for different literature studies.

Nanoparticle	**Examples**	**Remarks**	**References**
Carbon-based	CNT*, graphene, MWCNT**, fullerene	Greater thermal conductivity, inertness, and stability	[7]
Core-shell	Ag/SiO_2, Au/SiO_2, Ni/SiO_2, Fe_3O_4/SiO_2, Au/TiO_2, Fe/C, $FeNi/SiO_2$, ZnO/SiO_2	Better multi-functionality and greater stability	[46]
Hybrid	FeMo, CuMo	Active catalysis in combination	[50]
Metal/non-metal oxide	TiO_2, Fe_3O_4, ZnO, CaO, SiO_2, Al_2O_3	increased melting point and thermal stability	[46]
Metallic	Ni, Ag, Au, Rh, Pd, Pt	Moderate temperature stability and increased catalytic activity	[70]
* CNT: Carbon nanotubes; ** MWCNT: Multi-walled carbon nano tubes.			

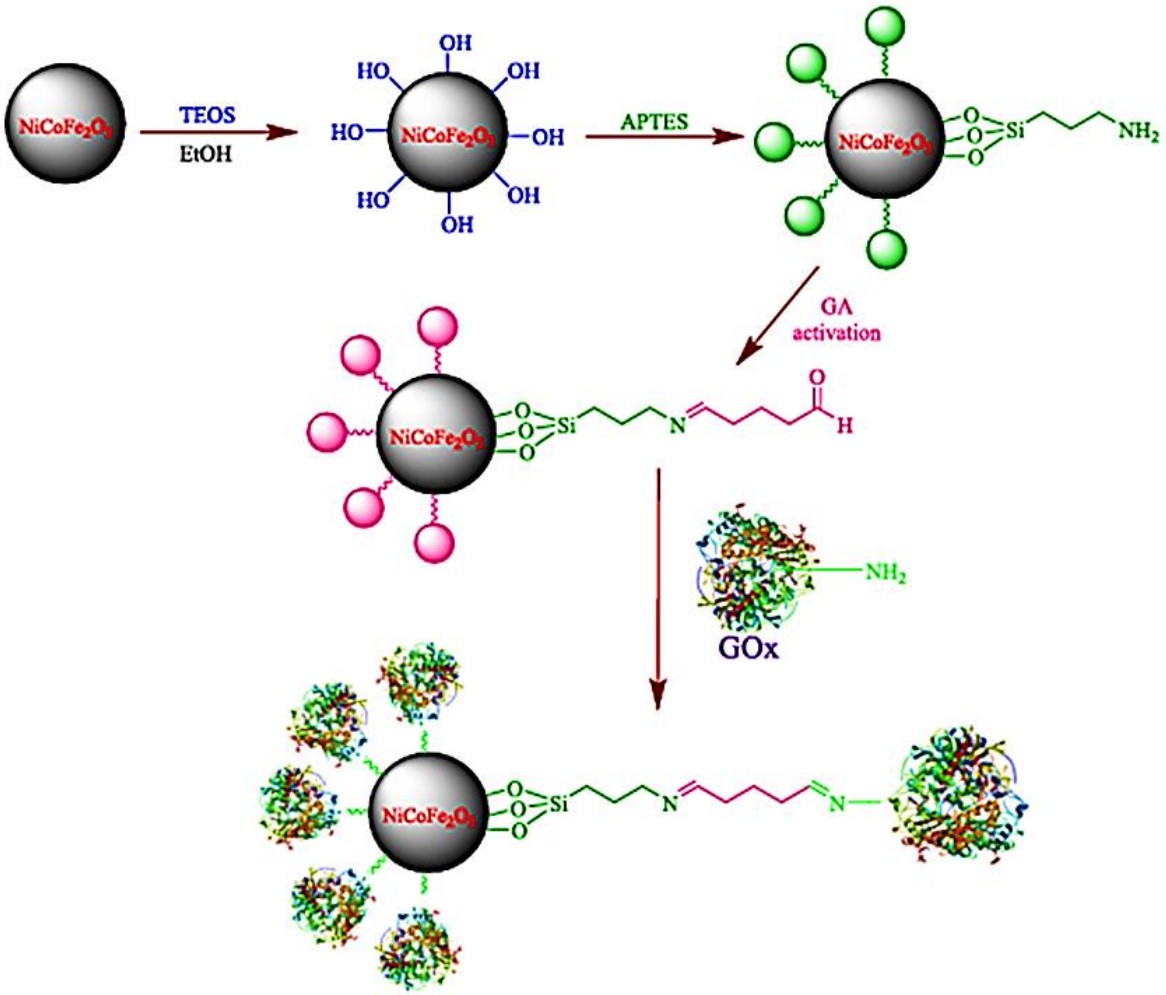

Figure 5. The immobilization of the GOx enzyme on Ni−Co-Fe_2O_4 NCs coated with SiO_2 utilizing gluconic acid (GA) as a cross-linker is depicted in this schematic picture (adopted from Nasir et al., [93]).

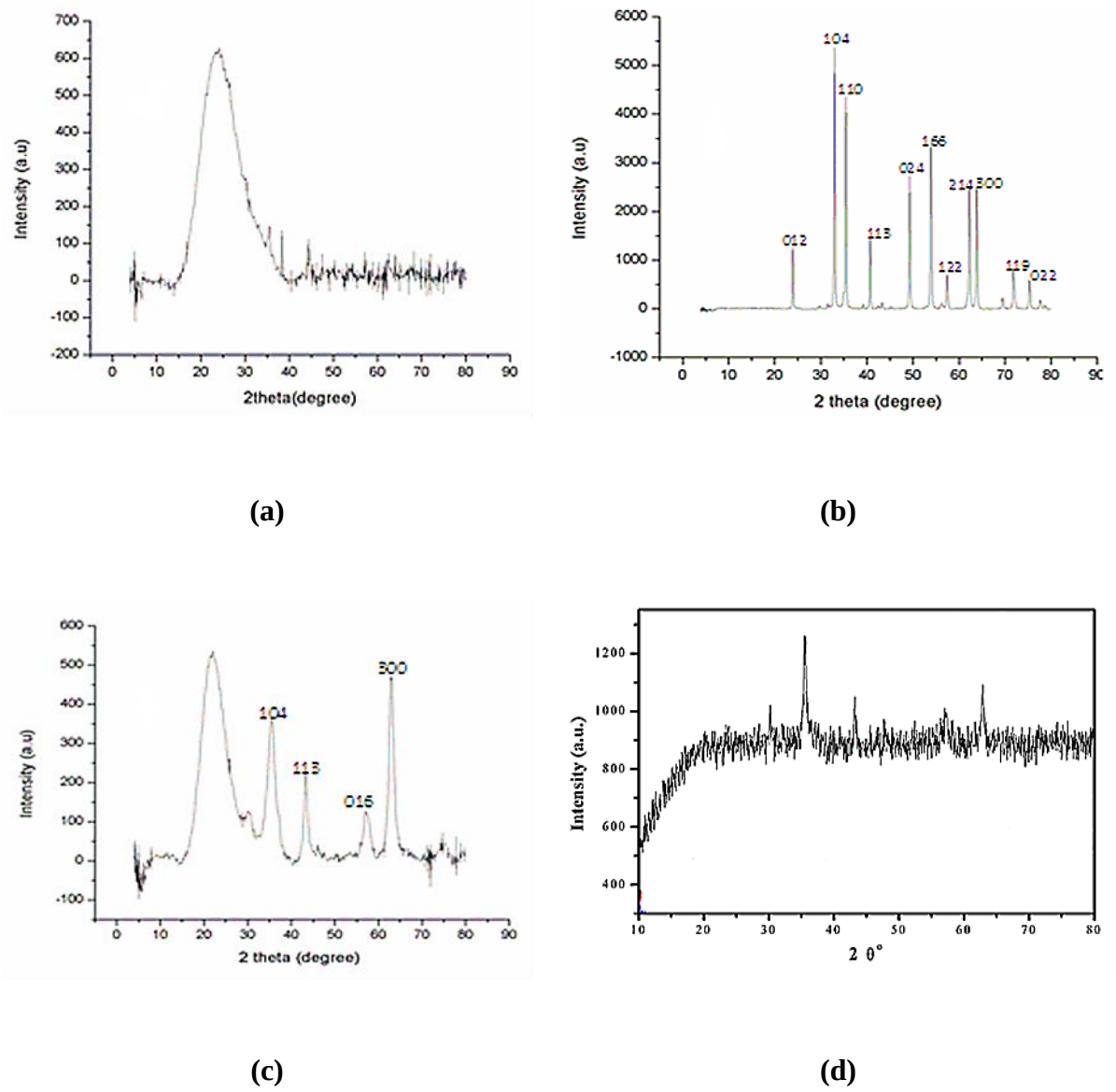

Figure 6. XRD patterns of **(a)** Fe_2O_3 NCs **(b)** SiO_2 NCs **(c)** Fe_2O_3/SiO_2 MNCs before photocatalytic degradation process, and **(d)** GOx enzymatic nano-catalysts on coated with Fe_2O_3/SiO_2 MNCs after photocatalytic degradation process.

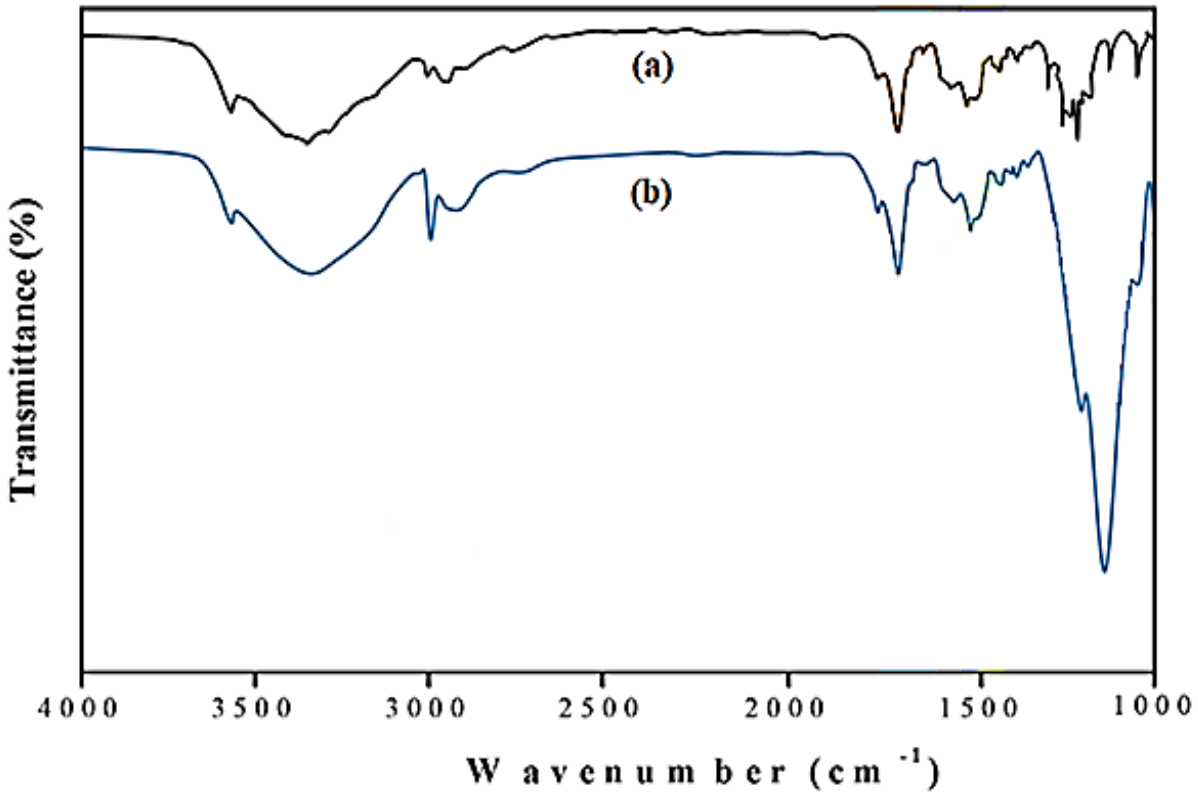

Figure 7. FTIR spectra of **(a)** pure GOx enzymatic nano-catalysts and, **(b)** immobilized Fe_2O_3 MNCs coated with SiO_2 NCs.

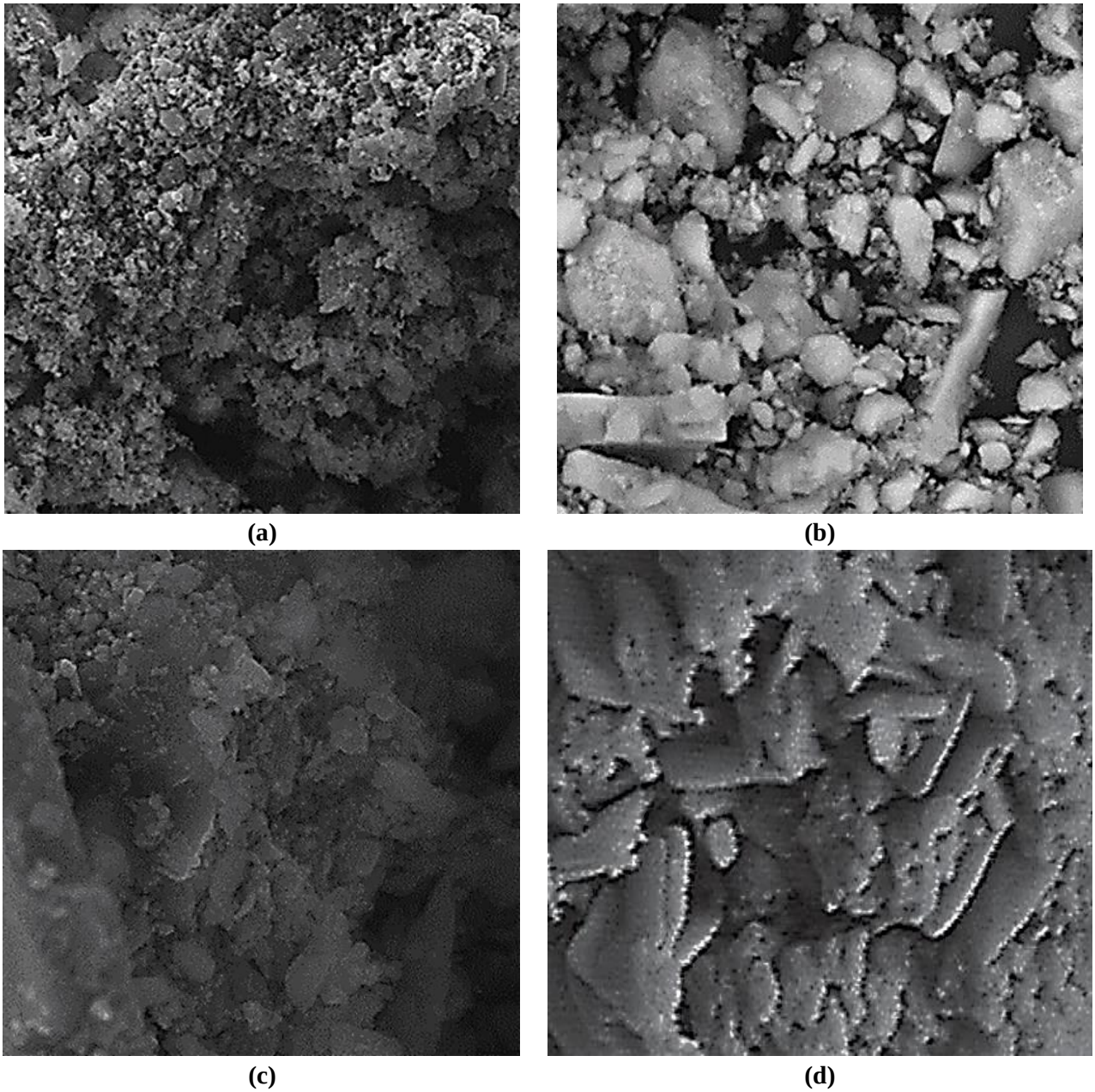

Figure 8. FESEM images of **(a)** Fe_2O_3 NCs, **(b)** SiO_2 NCs, **(c)** Fe_2O_3/SiO_2 MNCs before photocatalytic degradation process, and **(d)** Fe_2O_3/SiO_2 MNCs after photocatalytic degradation process (FESEM images size: 20 μm).

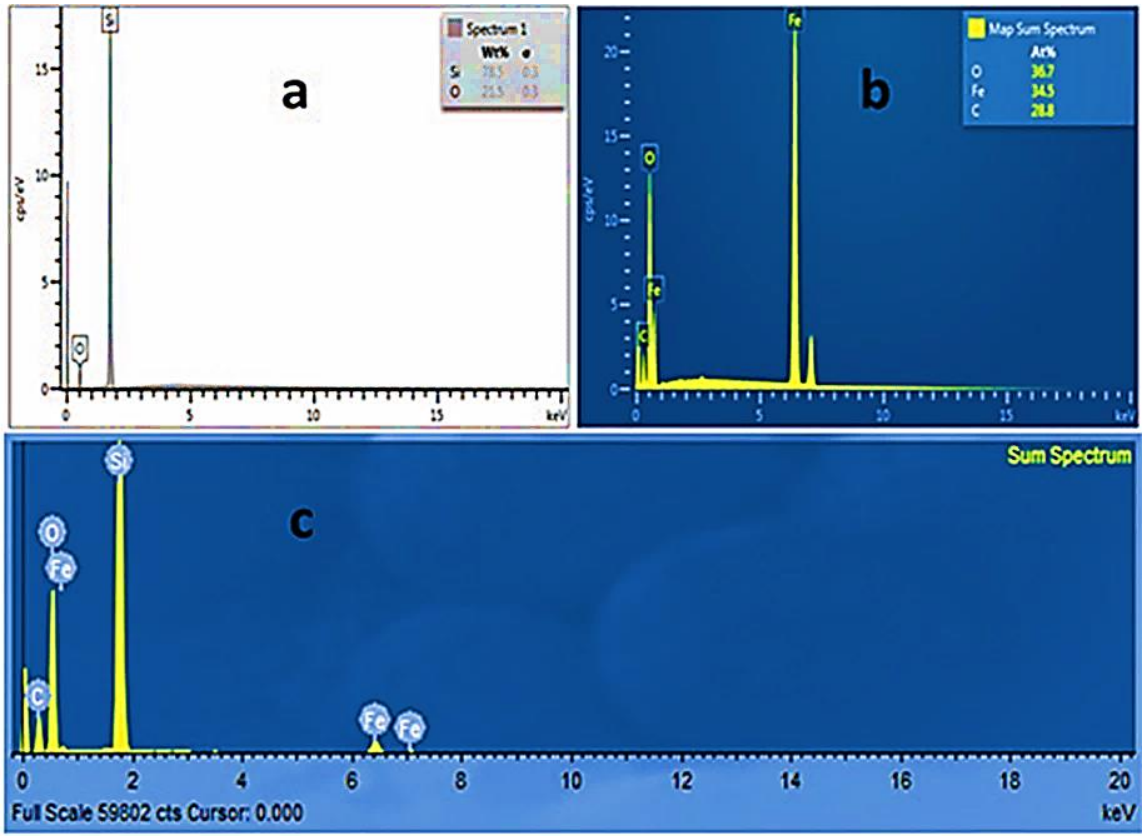

(a), (b), (c)

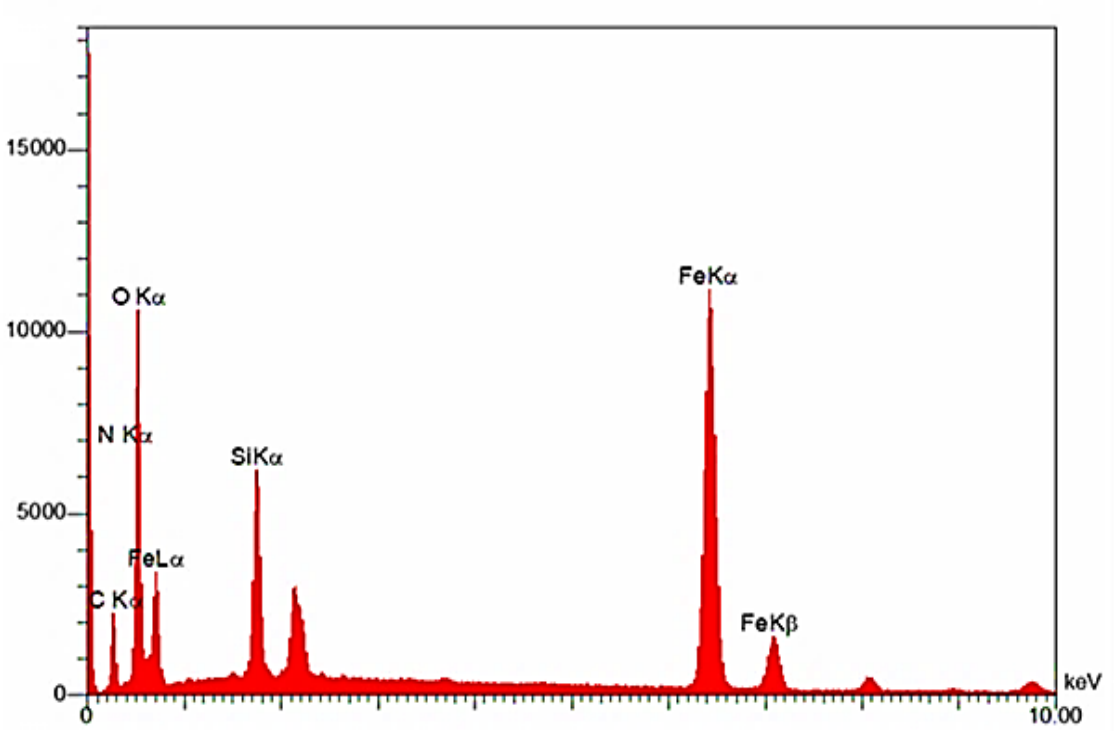

(d)

Figure 9. EDX images of **(a)** SiO_2 NCs, **(b)** Fe_2O_3 NCs, **(c)** Fe_2O_3/SiO_2 MNCs (before photocatalytic degradation process, and **(d)** Fe_2O_3/SiO_2 MNCs after photocatalytic degradation process, respectively.

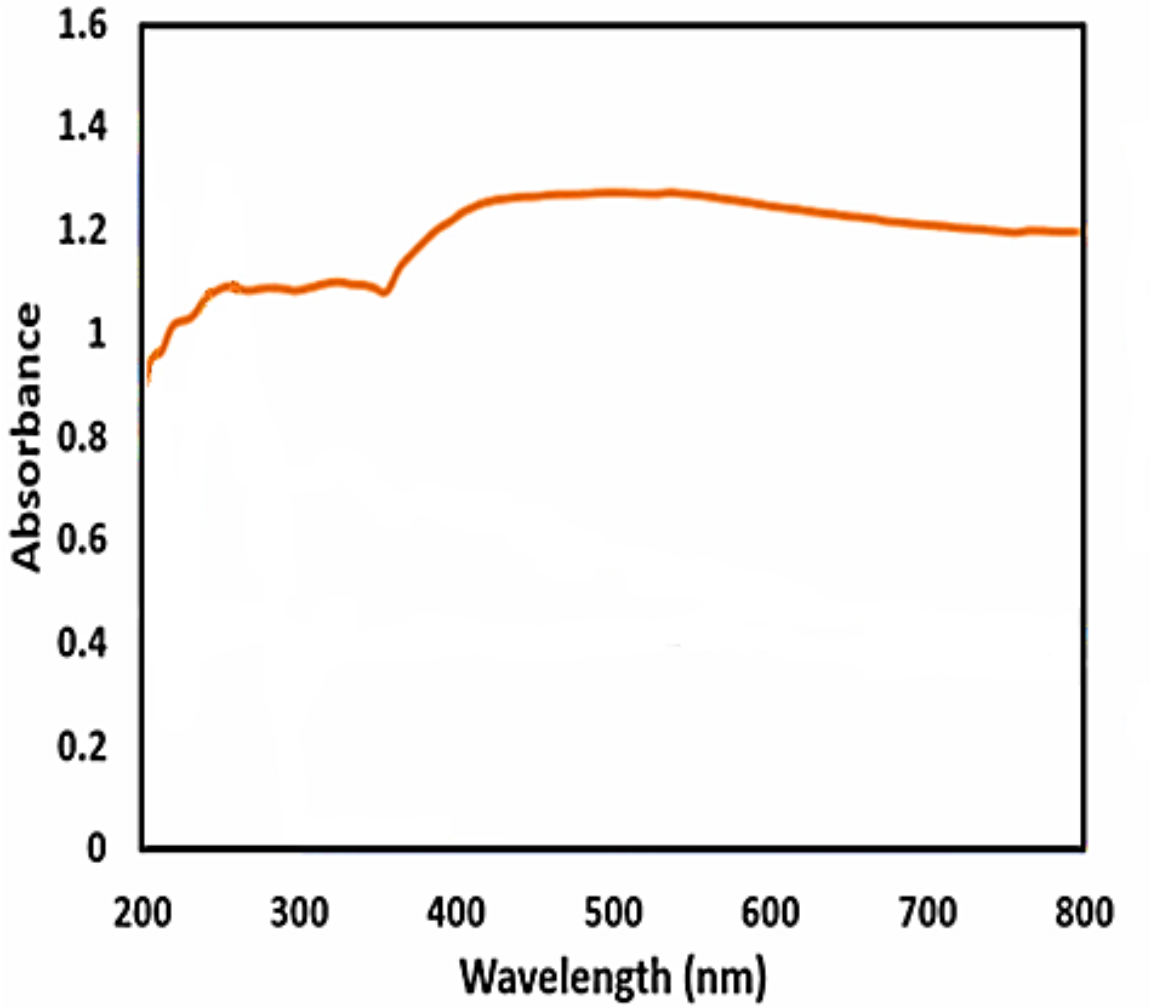

Figure 10. UV– vis spectra of Fe_2O_3/SiO_2 MNCs.

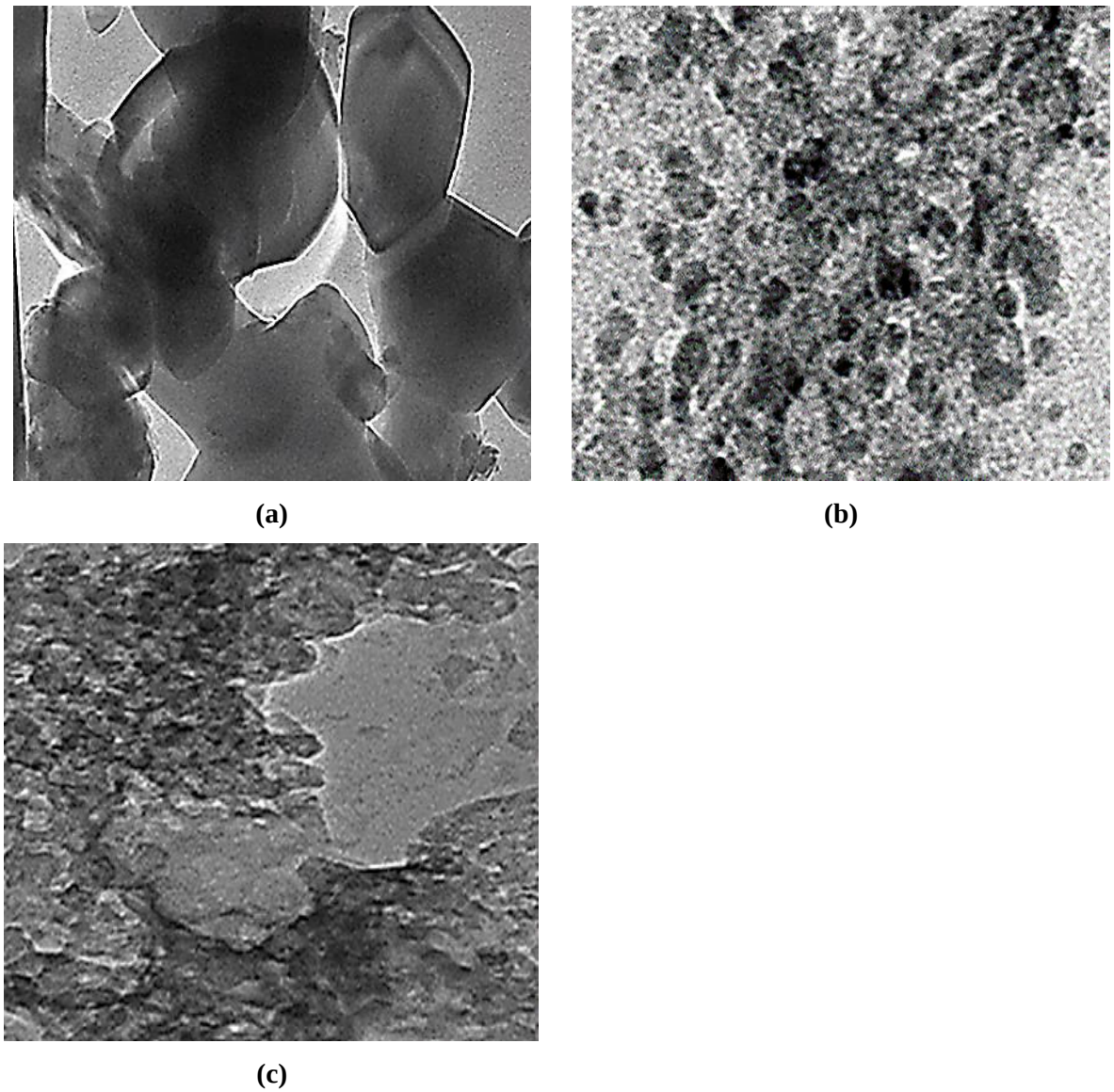

Figure 11. HRTEM images of Fe_2O_3/SiO_2 MNCs (a) before photocatalytic degradation process, **(b)** without immobilized GOx enzymatic nano-catalysts, and **(c)** with immobilized GOx enzymatic nano-cataylsts, respectively. (HRTEM image size: 100 nm).

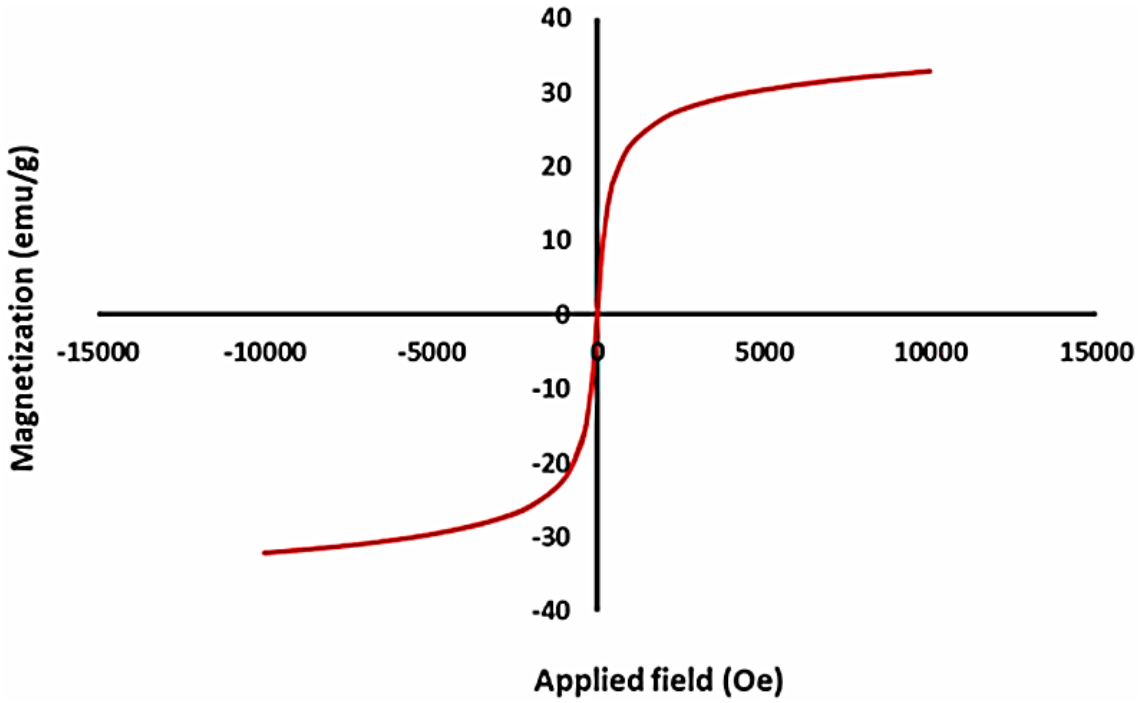

Figure 12. The VSM of Fe_2O_3/SiO_2 MNCs.

Table 9. The effect of photocatalytic degradation time with photocatalytic degradation process for GOx enzymatic nano-catalysts immobilized Fe_2O_3/SiO_2 MNCs.

Parameters	**Photocatalytic Degradation Efficiencies (%)**				
Photocatalytic Degradation Time (min)	**30 min (%)**	**60 min (%)**	**90 min (%)**	**120 min (%)**	**150 min (%)**
	52.67%	71.33%	91.54%	99.11%	97.50%

Table 10. The effect of photocatalytic temperatures with photocatalytic degradation process for GOx enzymatic nano-catalysts immobilized Fe_2O_3/SiO_2 MNCs.

Parameters	**Photocatalytic Degradation Efficiencies (%)**			
Photocatalytic Temperatures	**25ºC (%)**	**50ºC (%)**	**75ºC (%)**	**100ºC (%)**
	54.68%	99.45%	74.32%	50.14%

Table 11. The effect of pH values with photocatalytic degradation process for GOx enzymatic nano-catalysts immobilized Fe_2O_3/SiO_2 MNCs.

Parameters	**Photocatalytic Degradation Efficiencies (%)**			
pH Values	**pH=5.0 (%)**	**pH=7.0 (%)**	**pH=9.0 (%)**	**pH=11.0 (%)**
	75.83%	99.36%	96.50%	94.05%

Table 12. The effect of Fe_2O_3/SiO_2 MNCs concentrations with photocatalytic degradation process for GOx enzymatic nano-catalysts immobilized Fe_2O_3/SiO_2 MNCs.

Parameters	**Photocatalytic Degradation Efficiencies (%)**				
Fe_2O_3/SiO_2 MNCs concentrations	**5 mg/l (%)**	**10 mg/l (%)**	**15 mg/l (%)**	**20 mg/l (%)**	**25 mg/l (%)**
	51.07%	76.05%	89.17%	99.69%	97.94%

Table 13. The effect of GOx enzymatic nano-catalysts concentrations with photocatalytic degradation process for GOx enzymatic nano-catalysts immobilized Fe_2O_3/SiO_2 MNCs.

Parameters	**Photocatalytic Degradation Efficiencies (%)**			
GOx enzymatic nano-catalysts concentrations	**0.1 mg/l (%)**	**0.5 mg/l (%)**	**1.0 mg/l (%)**	**2.0 mg/l (%)**
	49.08%	73.45%	99.04%	97.38%

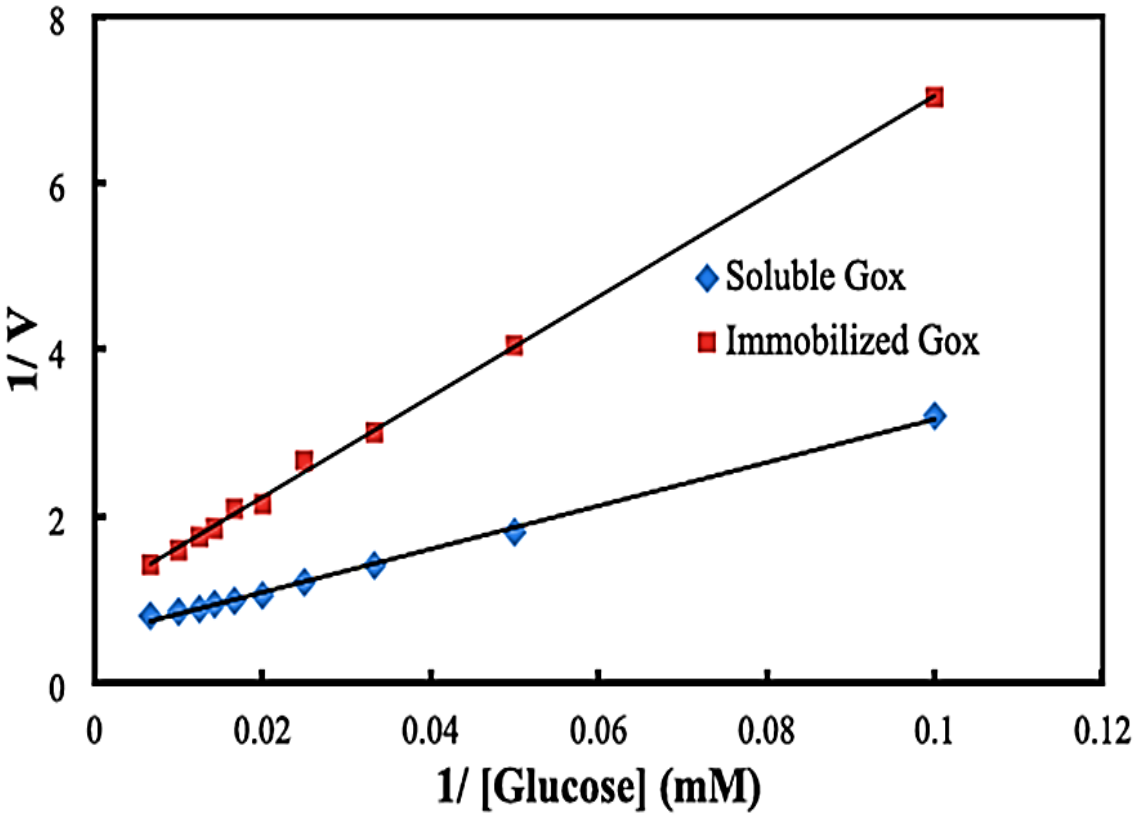

Figure 13. For soluble and immobilized GOx enzymatic nano-catalysts, double reciprocal plots.

Table 14. The kinetic parameters of free and immobilized GOx enzymatic nano-catalysts.

GOx Enzymatic Nano-Catalysts	**K_m (mM)**	**V_{max} (µmol/min)**	**V_{max} / K_m**	**Relative Activity (%)**
Free	45.29	1745.24	0.039	100
Immobilized	58.30	969.95	0.017	44.42